EXPERIMENTAL STUDY OF SEISMIC RESPONSE OF BUILDINGS WITH SUPPLEMENTAL FLUID DAMPERS

by

M.C. Constantinou, M.D. Symans

State University of New York
Department of Civil Engineering
Buffalo, NY 14260

THE STRUCTURAL DESIGN OF TALL BUILDINGS, Vol. 2, 93–132 (1993)

EXPERIMENTAL STUDY OF SEISMIC RESPONSE OF BUILDINGS WITH SUPPLEMENTAL FLUID DAMPERS

M. C. CONSTANTINOU AND M. D. SYMANS
Department of Civil Engineering, State University of New York, Buffalo, N Y 14260, U.S.A.

SUMMARY

This paper presents the results of an experimental study of the seismic response of buildings with supplemental fluid damping devices. These devices operate on the principle of fluid flow through orifices specially shaped so as to produce damping forces proportional to the velocity, i.e. the devices operate as linear viscous dampers. The experimental results demonstrate that the addition of fluid dampers to the tested steel model structure resulted in reductions of interstory drifts, floor accelerations and story shear forces by factors of two to three in comparison with the response of the same structure without the dampers.

1. INTRODUCTION

The conventional approach towards seismic hazard mitigation is to resist earthquakes through a combination of strength, deformability and energy absorption capability. The energy absorption capability of structures is typically low unless they are deformed inelastically. Commonly, structures are designed to absorb earthquake energy through localized damage of their lateral force resisting system.

An alternative approach has been advanced recently that introduces energy dissipating devices within the structural system and prevents the development of damage to the structural system. The means by which energy is dissipated in these added mechanical devices includes the yielding of mild steel,[1–3] sliding friction,[4–9] viscoelastic action in rubber-like materials[5,10–12] and fluid orificing.[13] A critical review of the various energy absorbing systems has been provided by the authors in a report[13] and in an accompanying paper in this journal.

Attaching energy dissipating devices to moment resisting frames reduces drift and thus bending moment in the columns. However, they change the behavior of the structural system to that of a braced frame. Accordingly, they introduce additional axial forces in the columns.[13] In devices with hysteretic behavior, such as friction and yielding steel dampers and devices with viscoelastic behavior, the additional axial forces in the columns are completely or partially in-phase with the peak bending moment. In contrast, purely viscous devices introduce axial force with its peak value being out-of-phase with the peak bending moment. As explained in Reference 13, this difference in behavior among energy dissipating devices is of importance in the design of damped tall structures.

This paper describes an experimental study of the seismic response of structures with supplemental fluid dampers that exhibit essentially linear viscous behavior. The mechanical characteristics of these devices are experimentally obtained over a wide range of frequencies of motion and of temperature. Shake table tests of a series of structural models are reported. Mathematical models that describe the behavior of the devices are presented and experimentally verified.

1062–8002/93/020093–40$25.00

Received 1 January 1993
Revised 1 March 1993

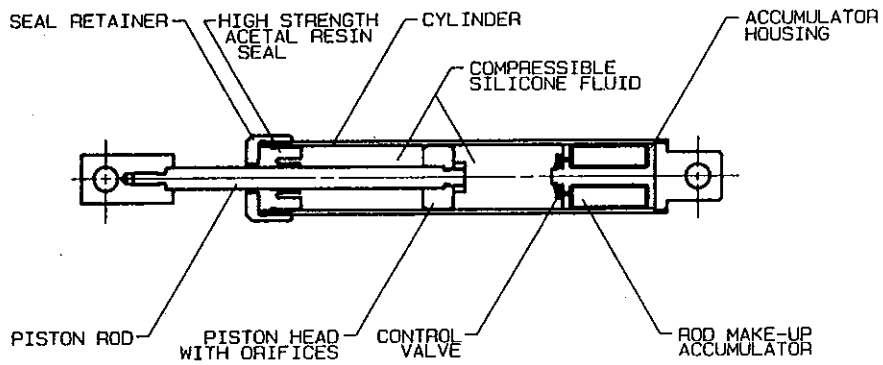

Figure 1. Construction of fluid viscous damper

2. DESCRIPTION OF DAMPERS

Damping devices that utilize fluid flow through orifices were originally developed for use as energy absorbing buffers on overhead cranes and then extensively used for the shock isolation of military hardware. The construction of the device tested is shown in Figure 1. It consists of a stainless steel piston, with a bronze orifice head and an accumulator. It is filled with silicone oil. The orifice flow is compensated by a passive bi-metallic thermostat that allows operation of the device over a temperature range of $-40°F$ to $160°F$ ($-40°C$ to $70°C$).

The force generated by the fluid damper is due to a pressure differential across the piston head. During motion of the piston head, the fluid volume is changed by the product of travel and piston rod area. Since the fluid is compressible, this change in fluid volume is accompanied by the development of a spring-like restoring force. This is prevented by the use of the accumulator. The tested device showed no measurable stiffness for piston motions with frequency less than about 4 Hz. In general, this cut-off frequency depends on the design of the accumulator and may be specified in the design.

The existence of the aforementioned cut-off frequency is a desirable property. The devices may provide additional viscous-type damping to the fundamental mode of the structure (typically with a frequency less than the cut-off frequency) and additional damping and stiffness to the higher modes. This may, in effect, completely suppress the contribution of the higher modes of vibration.

Typical fluid dampers utilize cylindrically-shaped orifices (known as 'square law' or 'Bernoullian' orifices). Such orifices produce damper forces proportional to the square of the velocity of the piston rod, a usually unacceptable performance in shock isolation. The orifice design in the tested fluid damper produces a force that is not proportional to velocity squared. The orifice utilizes a series of specially shaped passages to alter flow characteristics with fluid speed. A schematic of this orifice is shown in Figure 2. It is known as a 'fluidic control orifice'. It provides forces proportional to $|\dot{u}|^{\alpha}$, where α is a predetermined coefficient in the range 0·5 to 2·0. In earthquake engineering applications, a design with $\alpha = 1$ appears to be the most desired. It results in essentially linear viscous behavior. The devices utilized in this testing program were designed to have this behavior.

The mechanical characteristics of the dampers have been determined using a testing arrangement in which a hydraulic actuator applied a dynamic force along the axis of the damper. The force needed to maintain a specified motion of the damper piston rod was measured by a

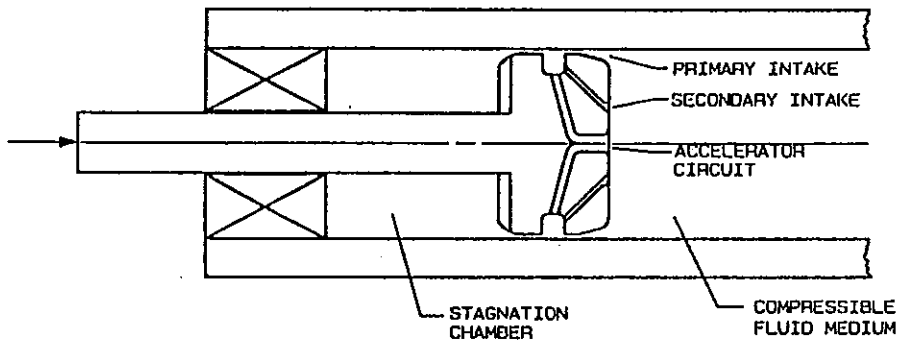

Figure 2. Fluidic control orifice

load cell which was connected between the damper and a reaction frame. The recorded force–displacement relationship was used to extract the mechanical characteristics of the dampers.

The frequency and amplitude of the motion of the damper piston was specified for each test. The actuator was run under displacement control such that the resulting motion of the damper piston was sinusoidal. The damper motion is given by

$$u = u_0 \sin(\omega t) \tag{1}$$

where u_0 is the amplitude of the displacement, ω is the frequency of motion, and t is the time. For steady-state conditions, the force needed to maintain this motion is

$$P = P_0 \sin(\omega t + \delta) \tag{2}$$

where P_0 is the amplitude of the force and δ is the phase angle. The area within the recorded force–displacement loops can be measured to determine the energy dissipated in a single cycle of motion

$$W_d = \oint P \, du = \pi P_0 u_0 \sin(\delta) \tag{3}$$

Introducing the quantities

$$K_1 = \frac{P_0}{u_0} \cos(\delta), \quad K_2 = \frac{P_0}{u_0} \sin(\delta) \tag{4}$$

where K_1 is the storage stiffness and K_2 is the loss stiffness, (2) may be written as

$$P = K_1 u + \frac{K_2}{\omega} \dot{u} \tag{5}$$

In this equation, the first term represents the force due to the stiffness of the damper, which is in phase with the motion, and the second term represents the force in the damper due to the viscosity of the damper, which is 90° out of phase with the motion. The damping coefficient is given by

$$C = \frac{K_2}{\omega} \tag{6}$$

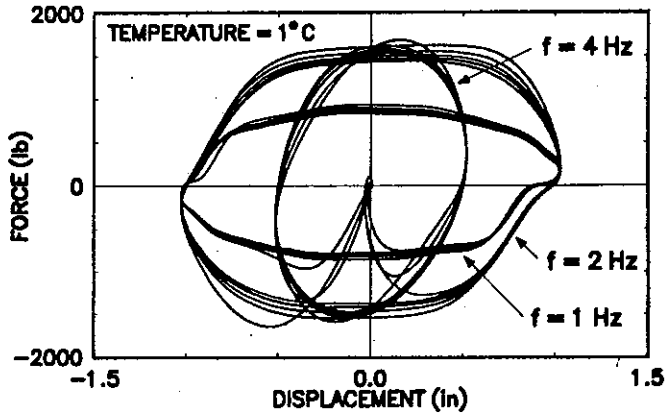

Figure 3. Recorded force–displacement loops at low temperature (1 in = 25·4 mm; 1 lb = 4·45 N)

The loss stiffness and phase angle are determined from (3) and (4) to be

$$K_2 = \frac{W_d}{\pi u_0^2} \tag{7}$$

$$\delta = \sin^{-1}\left(\frac{K_2 u_0}{P_0}\right) \tag{8}$$

Equations (4) and (6) through (8) were used to obtain the mechanical properties of the damper from experimentally measured values of W_d, P_0 and u_0. A total of 58 tests were conducted in the frequency range 0·1 to 25 Hz, peak velocity range 0·65 in s^{-1} to 18·2 in s^{-1} (16·5 to 462·3 mm s^{-1}) and at three temperatures: about 0°C, room temperature (about 22°C), and about 50°C. In all tests, five cycles were completed. The low-temperature tests were conducted with the damper encased in a plastic cylindrical tube containing a pack of ice with alcohol to lower the temperature. The high temperature tests were conducted with the damper encased in a cardboard cylindrical tube wrapped with teflon tape. A temperature adjustable heating unit was wrapped around the tube several times. The heat generated by the heating unit was transferred to the space between the damper and the cylindrical tube. In all cases, a thermocouple monitored the surface temperature of the housing of the device.

Typical recorded force–displacement loops are presented in Figures 3 through 5 at temperatures of 1°C, 23°C and 47°C and frequencies of 1, 2 and 4 Hz. In this range of frequency of motion, the device exhibits insignificant storage stiffness and its behavior is essentially linear viscous. At frequencies above about 4 Hz, the device exhibits storage stiffness reaching values approximately equal to the loss stiffness at frequencies exceeding 20 Hz. Figure 6 demonstrates this behavior in a test at a frequency of 20 Hz and an amplitude of 0·05 in (1·27 mm).

The mechanical properties of the device were found to be almost completely independent of the amplitude of motion. This was confirmed in tests conducted at the same frequency and different amplitude. Within a temperature range of about 0°C to 50°C, the device apparently exhibits a dependence of its mechanical properties on temperature, but this dependence is not significant.

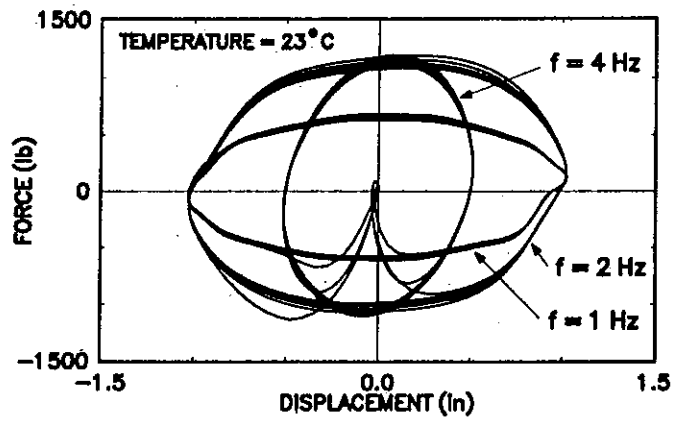

Figure 4. Recorded force–displacement loops at room temperature (1 in = 25·4 mm; 1 lb = 4·45 N)

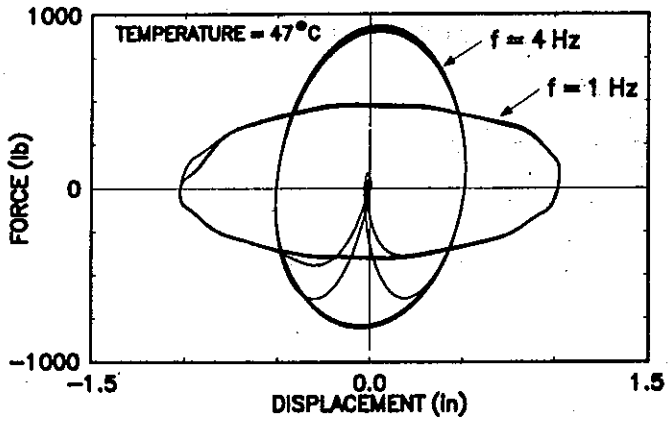

Figure 5. Recorded force–displacement loops at high temperature (1 in = 25·4 mm; 1 lb = 4·45 N)

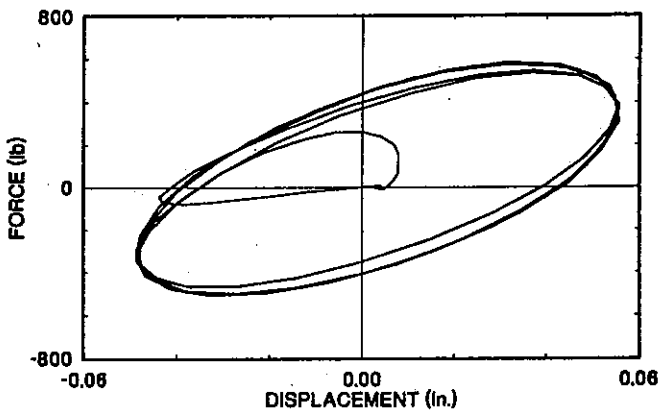

Figure 6. Recorded force–displacement loop at a frequency of 20 Hz and a temperature of 23°C (1 in = 25·4 mm; 1 lb = 4·45 N)

3. MATHEMATICAL MODELING OF DAMPERS

Over a large frequency range, the damper exhibits viscoelastic fluid behavior. The simplest model to account for this behavior is the Maxwell model.[14]

The Maxwell model is defined at the macroscopic level as

$$P + \lambda \dot{P} = C_0 \dot{u} \tag{9}$$

where λ is the relaxation time and C_0 is the damping constant at zero frequency. A more general Maxwell model may also be considered in which the derivatives are of fractional order:[15]

$$P + \lambda D^r[P] = C_0 D^q[u] \tag{10}$$

where $D^r[f(t)]$ is the fractional derivative of order r of the time dependent function f. For complex viscoelastic fluid behavior, Equation (10) may offer more control than (9) in modeling the behavior.

The generalized Maxwell model was considered initially. The parameter q was set equal to unity based on the assumption that the damping coefficient of the device is independent of the velocity over a wide range of values. For $q = 1$, the parameter C_0 becomes the damping constant at zero frequency. Parameters λ and r were then determined by fitting the curves of the experimental values of C and K_1 versus the frequency of motion. Analytical expressions for the mechanical properties are given by

$$K_1 = \frac{C_0 \lambda \omega^{1+r} \sin\left(\frac{\pi r}{2}\right)}{d} \tag{11}$$

$$C = \frac{K_2}{\omega} = \frac{C_0\left[1 + \lambda \omega^r \cos\left(\frac{\pi r}{2}\right)\right]}{d} \tag{12}$$

$$d = 1 + \lambda^2 \omega^{2r} + 2\lambda \omega^r \cos\left(\frac{\pi r}{2}\right) \tag{13}$$

$$\delta = \tan^{-1}\left(\frac{K_2}{K_1}\right) \tag{14}$$

The calibration of the model (10) was performed for the case of room temperature, for which experimental data over a wide frequency range were available. The calibration resulted in parameters $r = 1$, $q = 1$, $\lambda = 0{\cdot}006$ s and $C_0 = 88$ lb s in^{-1} (15·45 N s mm^{-1}). Interestingly, the calibrated model is the classical Maxwell model. A comparison of experimental and analytically derived properties of storage stiffness, damping coefficient and phase angle is presented in Figures 7 and 8. The comparison is very good except for frequencies above 20 Hz, where the model underpredicts the storage stiffness. Such frequencies are typically not considered in seismic analysis. Furthermore, the model predicts non-zero storage stiffness in the low frequency range (<2 Hz). The predicted storage stiffness is insignificant for practical purposes.

The damper exhibits a relaxation time of only 6 ms. This indicates that for low rates of damper force, the term $\lambda \dot{P}$ in (9) is insignificant. This occurs for frequencies below a cut-off value of about 4 Hz. Accordingly, for typical structural applications the term $\lambda \dot{P}$ may be neglected. The

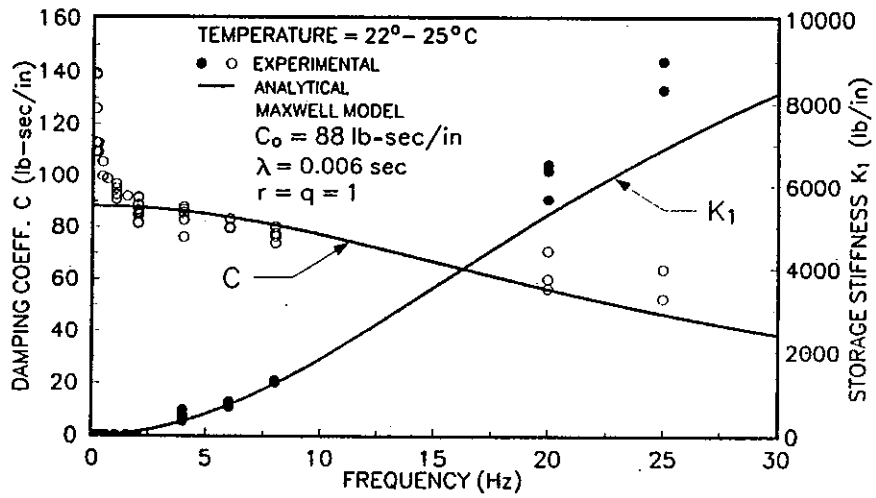

Figure 7. Comparison of experimental and analytically derived values of storage stiffness and damping coefficient at room temperature (1 in = 25·4 mm; 1 lb = 4·45 N)

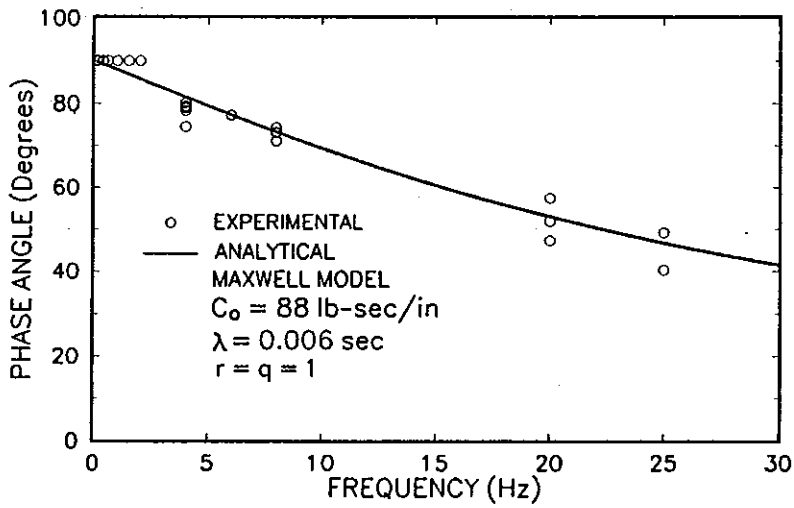

Figure 8. Comparison of experimental and analytically derived values of phase angle at room temperature (1 in = 25·4 mm; 1 lb = 4·45 N)

model of the damper below the cut-off frequency is simply

$$P = C_0\dot{u} \tag{15}$$

and, thus, for most practical purposes the damper behaves as a linear viscous dashpot.

The effect that temperature has on the single parameter of the model, C_0, is investigated in Figure 9. The recorded peak force in each test is plotted against the imposed peak velocity for the three values of temperature. It may be seen that the experimental results may be fitted to straight lines of slope C_0. For room temperature (24°C) and above, the behavior is indeed

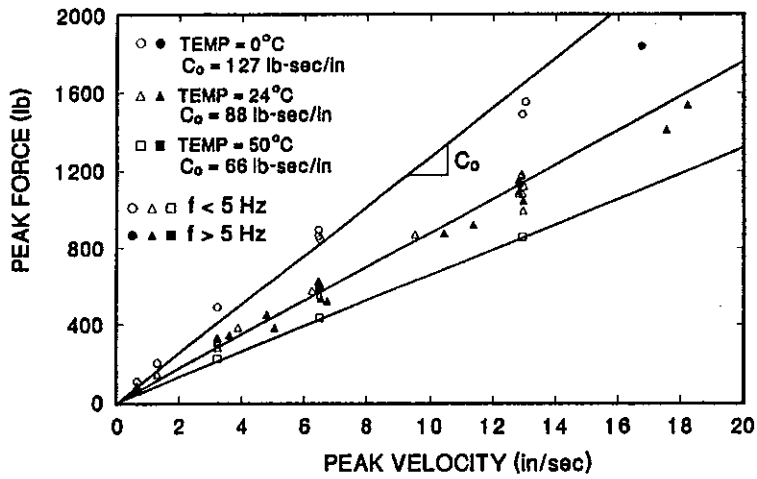

Figure 9. Recorded values of peak force versus peak velocity for low, room and high temperature tests (1 in = 25·4 mm; 1 lb = 4·45 N)

linear viscous to velocities of about 20 in s^{-1} (508 mm s^{-1}) and beyond. As temperature drops, the experimental results deviate from linearity at a lower velocity.

The values of the constant C_0 in Figure 9 demonstrate that the damper exhibits a stable behavior over a wide range of temperatures. Between about 0°C and 50°C, constant C_0 reduces by a factor of less than 2. Assuming that a design for a building application will be anchored at a temperature of about 24°C, variations of temperature in the range 0°C to 50°C will result in variations in the damping ratio of +44% to −25%. That is, if a design calls for a damping ratio of 20% of critical, extreme temperature variations will alter the damping ratio in the range of 15% to 29% of critical.

4. ONE-STORY AND THREE-STORY STEEL STRUCTURES

A series of tests was performed on a model structure (see Figure 10). The structure was a three-story 1:4 scale steel frame which modeled a shear building by the method of artificial mass simulation.[16] The model does not represent a similitude-scaled replica of a full-scale building. Rather, the test structure was designed as a small structural system. The model has been used in a number of previous earthquake simulation studies. The mass of each floor of the three-story model was 5·46 lb s^2 in^{-1} (958 kg) for a total mass of 16·38 lb s^2 in^{-1} (2874 kg). For some of the tests, the structure was modified by rigidly bracing the second and third stories so that the frame would act as a one-story structure. The one-story model had a total mass of 16·7 lb s^2 in^{-1} (2930 kg).

For the one-story structure, the dampers were placed at the first story and consisted of either two or four damping units (see Figure 11). For the three-story structure, the dampers were placed at the first story for the two and four damper cases and at all three stories for the six damper cases (see Figure 12).

Testing proceeded in the following sequence. First, the one-story configuration without and with fluid dampers was tested. The structure suffered damage in previous testing and exhibited both low stiffness and strength. Cracks existed on the webs of the structural tees forming the first story columns. Propagation of the cracks was prevented by drilling small holes at the tip

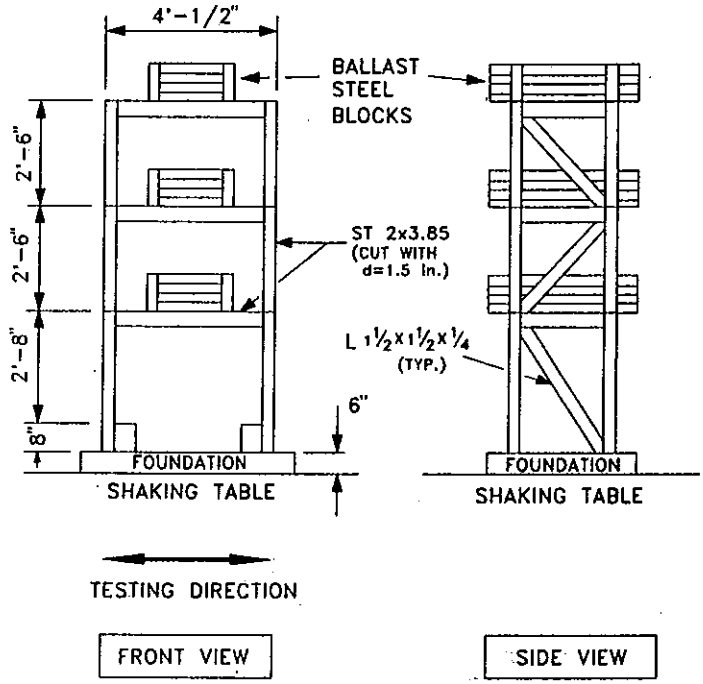

Figure 10. Schematic of model structure (1 in = 25·4 mm)

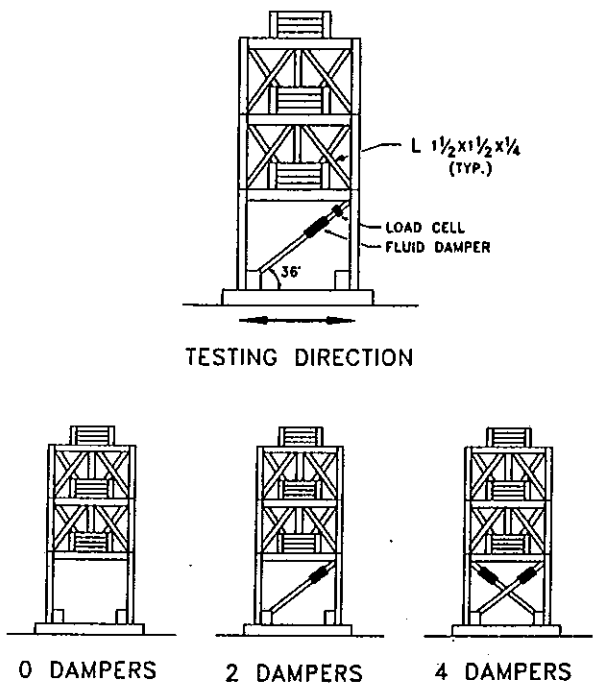

Figure 11. Damper configurations for one-story structure (1 in = 25·4 mm)

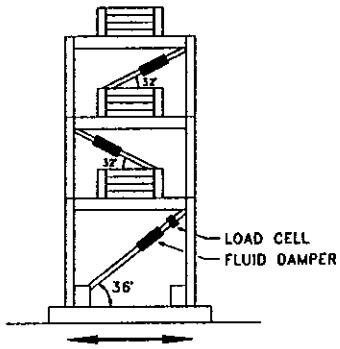

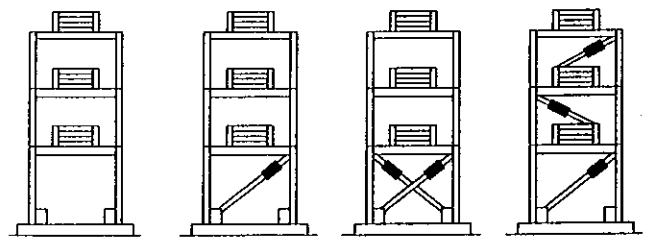

Figure 12. Damper configurations for three-story structure

of each crack. In this condition, the one-story structure was identified to have, at small amplitudes of vibration, a frequency of 2 Hz and damping ratio of 0·55% of critical. In seismic excitation, damping was estimated to be about 2% of critical.

Subsequently, the one-story structure was tested in a stiffer configuration. Steel plate stiffeners were welded at the top and bottom of each first-story column. The properties of the structure at small amplitudes of vibration were identified to have a frequency of 3·13 Hz and a damping ratio of 2% of critical. Under seismic excitation, damping was estimated at about 3% of critical. Tests were conducted in this one-story configuration both with and without fluid dampers.

Recognizing that damping in the structure without fluid dampers may be low, a different configuration was created and tested. A system of wire rope cables and pulleys was attached to the one-story stiffened structure as shown in Figure 13. The pulleys were locked so that during deformation the cables slid on the pulley guides. During motion, the cables did not change length so that they introduced frictional damping without increasing the stiffness. In seismic excitation, this damping was estimated to be about 5% of critical. In this configuration, tests were conducted without fluid dampers.

In the three-story configuration, the bracing of the top two stories was removed. The structure was identified at small amplitudes of motion to have a fundamental frequency of 2 Hz and a corresponding damping ratio equal to 1·74% of critical. Tests were conducted both with and without dampers.

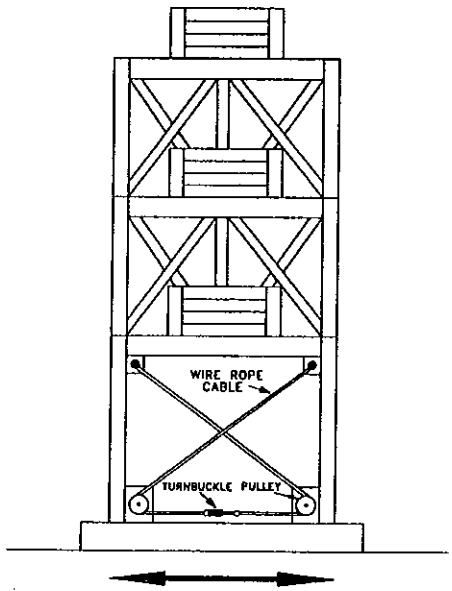

Figure 13. Schematic of structure with wire rope cables

5. TEST PROGRAM AND RESULTS

A total of 66 earthquake simulation tests were performed on the model structure. The earthquake signals and their characteristics are listed in Table I. Each record was compressed in time by a factor of two to satisfy the similitude requirements of the quarter-length scale model. As an example, Figure 14 shows recorded time histories of the table motion for the El Centro earthquake. The acceleration and displacement records were directly measured, whereas the velocity record was obtained by numerical differentiation of the displacement record. It may be observed that the peak ground motion was reproduced well, but not exactly, by the table generated motion. Figure 14 also shows the acceleration response spectrum of the table motion. This spectrum is compared with the spectrum of the actual record to demonstrate the good reproduction of the motion by the table.

The experimental results for the unstiffened and stiffened one-story structure are summarized in Tables II and III, respectively. For each test, the peak values of the table motion in the horizontal direction, the structural system conditions, and the excitation, are given. The excitation is identified with a percentage figure representing a scaling factor on the acceleration, velocity and displacement of the actual record. For example, the figure 200% denotes a motion scaled up by a factor of two in comparison with the actual record. The displacement and acceleration responses were measured directly, whereas the velocity response was determined by numerical differentiation of the displacement record. The peak drift is given as a percentage of the story height which was 32 in (813 mm). In addition, the peak drift has been determined based upon the horizontal component of the damper displacement. There is a quantitative difference between the two values of the peak drift which has been attributed to slipping at the

Table I. Earthquake motions used in test program and characteristics in prototype scale (1 in = 25·4 mm)

Notation	Record	Magnitude	Predominant frequency range (Hz)	Peak acceleration (g)	Peak velocity (in s^{-1})	Peak displ. (in)
El Centro S00E	Imperial Valley, May 18, 1940, component S00E	6.7	1–4	0.34	13.17	4.28
Taft N21E	Kern County, July 21, 1952, component N21E	7.2	0.5–5	0.16	6.19	2.64
Pacoima S74W	San Fernando, February 9, 1971, component S74W	6.4	0.25–2	1.08	22.73	4.26
Miyagi-Ken-Oki	Tohoku University, Sendai, Japan, June 12, 1978, component EW	7.4	0.5–5	0.16	5.55	2.00
Hachinohe	Tokachi-Oki earthquake, Japan, May 16, 1968, component NS	7.9	0.25–1.5	0.23	14.06	4.68

bolted connections between the structural frame and the lateral bracing. The peak base shear was calculated from the known masses and recorded accelerations and is given as a fraction of the total weight (6446 lb or 28743 N) of the structure.

Results in graphical form for some tests are presented in Figures 15 to 19. The figures present recorded loops of base shear force over weight ratio versus the first-story drift. Furthermore, for each test, the figures also present the contributions to the base shear from the fluid dampers and the columns. It is evident in these graphs that the contribution from the fluid dampers to the base shear–drift loops is purely of a viscous nature and accordingly the dampers display no stiffness. This confirms that the additional column axial load due to the damper forces occurs out of phase with the peak drift so that column compression failure is not a concern. Furthermore, Figure 16 illustrates response to only horizontal motion whereas Figure 17 presents the response to both horizontal and vertical input motion.

The experimental results for the three-story structure tests are given in Table IV. For each test, the peak values of the table motion in the horizontal direction are given. The peak drift is given as a percentage of the story height which was 32 in (813 mm) for the first story and 30 in (762 mm) for the second and third stories. In addition, the peak drift of the first story has been determined based upon the horizontal component of the damper displacement. The quantitative difference between the two values is again a result of slipping at the bolted connections between the structural frame and the lateral bracing. The peak acceleration at each floor is given and the peak shear force at each story is given as a fraction of the total weight (6332 lb or 28235 N) of the structure. Plots of recorded story shear force over total weight ratio versus story drift for some tests are presented in Figures 20 to 22.

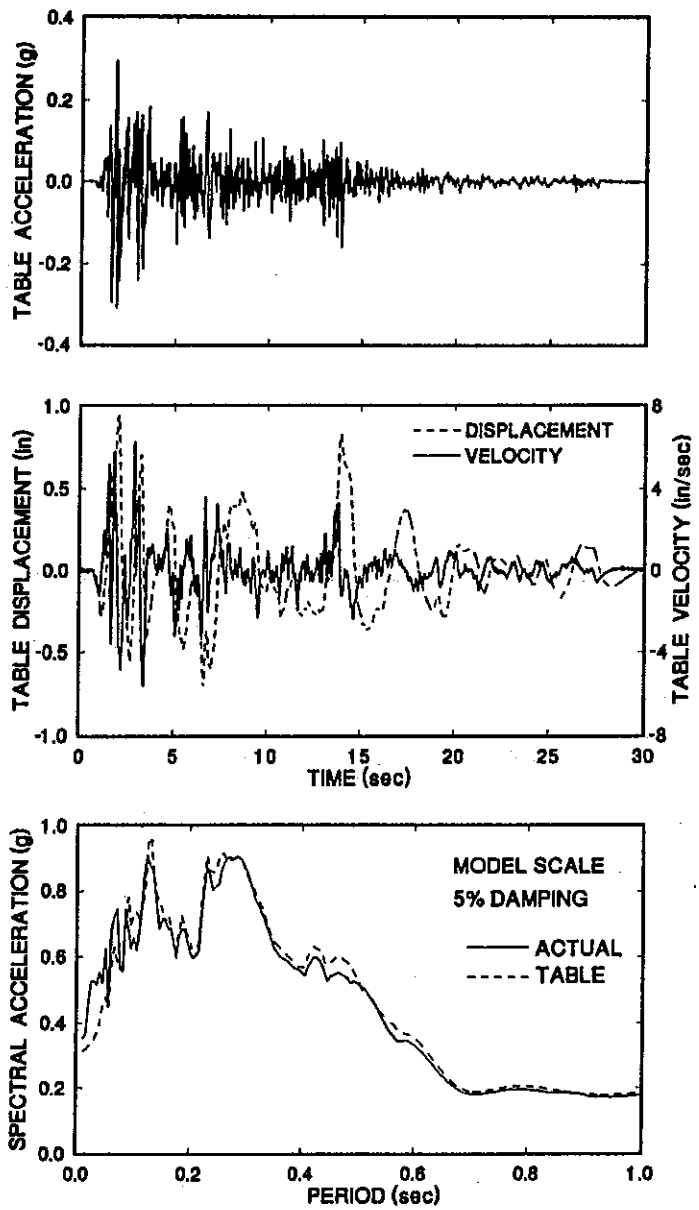

Figure 14. Time histories and displacement, velocity and acceleration and spectral acceleration and displacement of shaking table excited with El Centro 100% motion (1 in = 25·4 mm)

A number of observations related to the effectiveness of fluid dampers are made from the results of Tables II through IV and from Figures 15 to 22. A comparison of responses between the one-story structure both with and without fluid dampers reveals ratios of peak story drift in the damped structure to peak story drift in the undamped moment-resisting frame structure, RD, in the range 0·3 to 0·7 and ratios of peak base shear force in the damped structure to peak base shear force in the undamped structure, RBS, in the range 0·4 to 0·7. These significant

Table II. Summary of experimental results for unstiffened one-story structure (1 in = 25·4 mm)

Test	Excitation	DMP	System parameters		Peak table motion (Horiz.)			Peak base shear / weight	Peak drift / height (%)	Peak drift† / height (%)
			f (Hz)	ξ (%)	Displ. (in)	Veloc. (in s^{-1})	Accel. (g)			
1	El Centro 10%	0	2·00‡	0·55§	0·093	0·656	0·038	0·085	0·623	—
2	El Centro 20%	0	2·00‡	0·55§	0·188	1·259	0·071	0·160	1·205	—
3	El Centro 33·3%	0	2·00‡	0·55§	0·310	2·022	0·107	0·228	1·842	—
4	Taft 33·3%	0	2·00‡	0·55§	0·185	0·838	0·044	0·091	0·688	—
5	Taft 66·7%	0	2·00‡	0·55§	0·374	1·666	0·097	0·153	1·134	—
6	Taft 100%	0	2·00‡	0·55§	0·562	2·475	0·144	0·224	1·740	—
7	Taft 100%	2	2·04	28·4	0·563	2·491	0·151	0·129	0·724	0·689
8	Taft 100% (H&V)	2	2·04	28·4	0·566	2·491	0·148	0·130	0·775	0·702
9	El Centro 33·3%	2	2·04	28·4	0·309	2·125	0·106	0·087	0·500	0·469
10	El Centro 66·7%	2	2·04	28·4	0·618	4·009	0·197	0·168	1·071	0·997
11	El Centro 100%	2	2·04	28·4	0·947	6·275	0·310	0·259	1·693	1·576
12	Miyagiken 100%	2	2·04	28·4	0·479	2·403	0·155	0·115	0·636	0·754
13	Miyagiken 200%	2	2·04	28·4	0·961	4·622	0·308	0·234	1·459	1·688
14	Hachinohe 50%	2	2·04	28·4	0·644	2·625	0·116	0·122	0·806	0·930
15	Hachinohe 100%	2	2·04	28·4	1·291	5·172	0·215	0·247	1·645	1·808
16	El Centro 100%	4	2·10	57·7	0·947	6·244	0·298	0·301	1·031	1·002
17	Taft 100%	4	2·10	57·7	0·562	2·491	0·145	0·115	0·504	0·467
18	Miyagiken 200%	4	2·10	57·7	0·962	4·613	0·305	0·200	0·870	0·815
19	Hachinohe 100%	4	2·10	57·7	1·290	5·272	0·216	0·214	1·114	1·026
20	Taft 200%	4	2·10	57·7	1·132	4·900	0·301	0·226	1·067	0·966
21	Taft 300%	4	2·10	57·7	1·700	7·428	0·476	0·342	1·667	1·514
22	El Centro 150%	4	2·10	57·7	1·418	9·509	0·487	0·456	1·563	1·402
23	Miyagiken 320%	4	2·10	57·7	1·635	7·822	0·536	0·338	1·564	1·307
24	Hachinohe 150%	4	2·10	57·7	1·938	7·959	0·319	0·321	1·742	1·490
25	Pacoima Dam 50%	4	2·10	57·7	0·598	5·556	0·452	0·278	1·155	0·993
26	Pacoima Dam 75%	4	2·10	57·7	0·897	8·409	0·658	0·412	1·755	1·626

DMP is the number of dampers.
f is the undamped frequency.
† indicates measured from component of damper displacement.
H&V are the horizontal and vertical components.
‡ 2·00 to 1·94 Hz depending on the amplitude of motion.
§ 0·55 to 2·2% depending on the amplitude of motion.

Table III. Summary of experimental results for unstiffened one-story structure (1 in = 25·4 mm)

Test	Excitation	DMP	System parameters		Peak table motion (Horiz.)			Peak base shear / weight	Peak drift / height (%)	Peak drift† / height (%)
			f (Hz)	ξ (%)	Displ. (in)	Veloc. (in s^{-1})	Accel. (g)			
50	El Centro 33·3%	0	3·13‡	2·0‡	0·318	2·138	0·110	0·300	0·970	—
51	Taft 100%	0	2·99‡	2·9‡	0·561	2·484	0·144	0·431	1·479	—
52	El Centro 33·3%	0§	3·15‡	4·8‡	0·318	2·134	0·112	0·276	0·853	—
53	Taft 100%	0§	3·17‡	5·1‡	0·561	2·516	0·147	0·307	0·944	—
54	El Centro 33·3%	2	3·27	19·3	0·318	2·094	0·110	0·203	0·635	0·547
55	El Centro 66·7%	2	3·27	19·3	0·632	4·222	0·199	0·393	1·230	1·101
56	Taft 100%	2	3·27	19·3	0·563	2·494	0·145	0·226	0·667	0·594
57	Taft 200%	2	3·27	19·3	1·129	4·912	0·300	0·424	1·362	1·228
58	Hachinohe 100%	2	3·27	19·3	1·289	5·234	0·215	0·263	0·858	0·725
59	Hachinohe 150%	2	3·27	19·3	1·935	7·900	0·324	0·383	1·262	1·118
60	El Centro 33·3%	4	3·35	37·4	0·320	2·084	0·114	0·173	0·441	0·372
61	El Centro 66·7%	4	3·35	37·4	0·632	4·178	0·201	0·335	0·874	0·779
62	El Centro 100%	4	3·35	37·4	0·947	6·281	0·304	0·485	1·305	1·186
63	Taft 100%	4	3·35	37·4	0·561	2·556	0·148	0·180	0·437	0·410
64	Taft 200%	4	3·35	37·4	1·129	4·972	0·304	0·342	0·920	0·819
65	Taft 300%	4	3·35	37·4	1·695	7·425	0·487	0·504	1·405	1·247
66	Hachinohe 150%	4	3·35	37·4	1·934	7·878	0·326	0·330	0·979	0·862

DMP is the number of dampers.
f is the undamped frequency.
† indicates measured from component of damper displacement.
‡ measured from hysteresis loop under seismic excitation.
§ wire rope cables attached to increase energy dissipation.

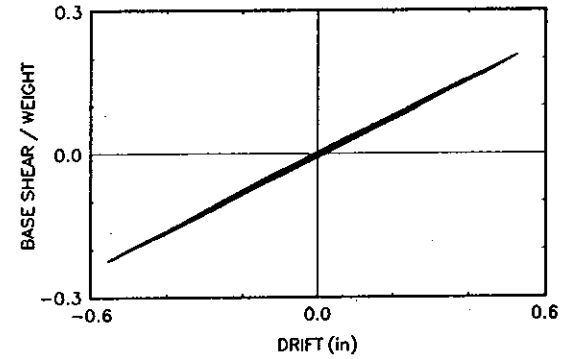

Figure 15. Experimental results for the one-story unstiffened structure with no dampers subjected to Taft 100% motion (1 in = 25·4 mm)

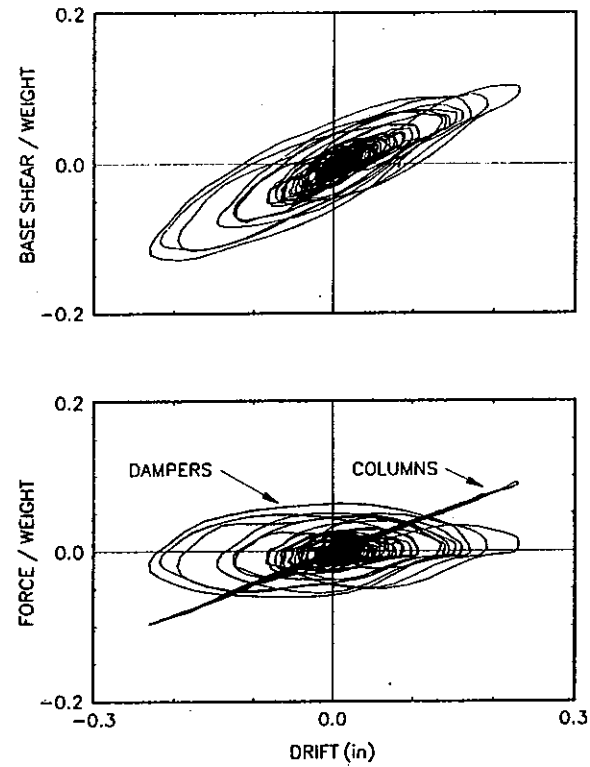

Figure 16. Experimental results for the one-story unstiffened structure with two dampers subjected to Taft 100% motion (1 in = 25·4 mm)

reductions in response are the result of increased ability to dissipate energy and are not the result of changes in stiffness.

The corresponding ratios of story drift and story shear force in the three-story structure are lower and typically in the range 0·3 to 0·5. The lower values of these ratios in the three-story

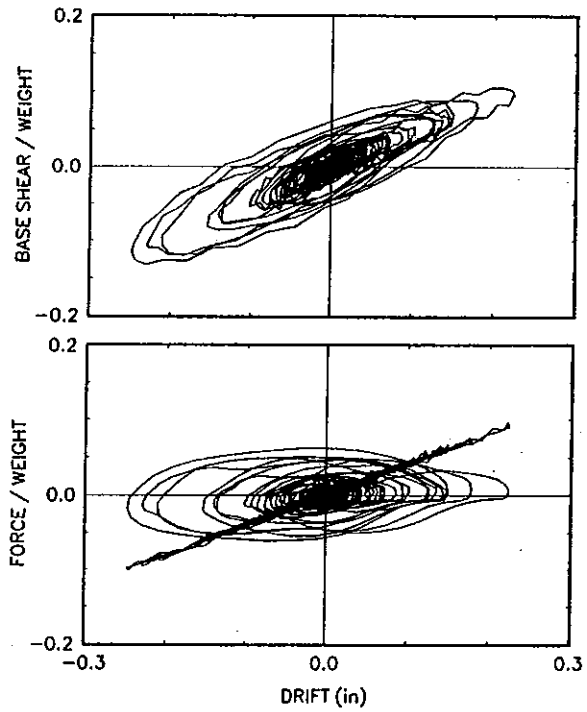

Figure 17. Experimental results for the one-story unstiffened structure with two dampers subjected to horizontal and vertical components of Taft 100% motion (1 in = 25·4 mm)

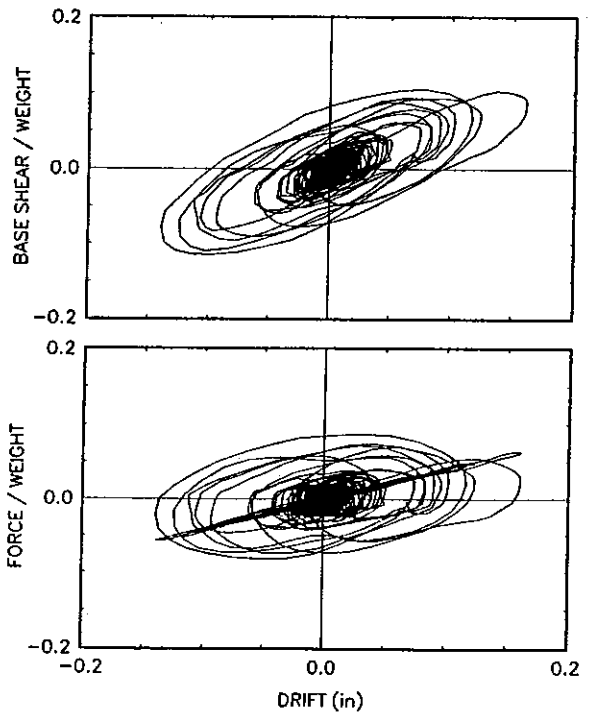

Figure 18. Experimental results for the one-story unstiffened structure with four dampers subjected to Taft 100% motion (1 in = 25·4 mm)

Table IV. Summary of experimental results for three story structure (1 in = 25·4 mm)

Test	Excitation	DMP	System parameters		Peak table motion (Horiz.)			Peak acceleration (g)		
			f (Hz)	ξ (%)	Displ. (in)	Veloc. (in s^{-1})	Accel. (g)	1st Floor	2nd Floor	3rd Floor
27	El Centro 33·3%	0	2·00‡	1·74‡	0·317	2·138	0·109	0·275	0·308	0·417
28	El Centro 50%	0	2·00‡	1·74‡	0·477	3·169	0·157	0·389	0·410	0·585
29	Taft 100%	0	2·00‡	1·74‡	0·562	2·472	0·146	0·424	0·403	0·555
30	El Centro 50%	6	2·03	19·4	0·475	3·134	0·152	0·127	0·152	0·205
31	El Centro 100%	6	2·03	19·4	0·949	6·322	0·312	0·205	0·286	0·368
32	El Centro 150%	6	2·03	19·4	1·419	9·447	0·485	0·340	0·402	0·534
33	Taft 100%	6	2·03	19·4	0·562	2·516	0·145	0·140	0·136	0·178
34	Taft 200%	6	2·03	19·4	1·131	4·994	0·300	0·253	0·264	0·348
35	Taft 300%	6	2·03	19·4	1·700	7·416	0·465	0·362	0·379	0·513
36	Hachinohe 100%	6	2·03	19·4	1·290	5·325	0·215	0·248	0·276	0·334
37	Miyagiken 200%	6	2·03	19·4	1·036	5·003	0·326	0·247	0·271	0·342
38	Pacoima Dam 50%	6	2·03	19·4	0·596	5·538	0·455	0·282	0·308	0·376
39	Pacoima Dam 50% (H&V)	6	2·03	19·4	0·555	5·244	0·419	0·273	0·314	0·377
40	El Centro 100% (H&V)	6	2·03	19·4	0·938	6·147	0·298	0·239	0·293	0·390
41	Taft 200% (H&V)	6	2·03	19·4	1·133	5·013	0·316	0·243	0·283	0·352
42	El Centro 50%	2	2·03	9·9	0·471	3·116	0·156	0·220	0·286	0·301
43	El Centro 75%	2	2·03	9·9	0·710	4·663	0·225	0·316	0·391	0·427
44	Taft 100%	2	2·03	9·9	0·563	2·541	0·147	0·172	0·218	0·271
45	Taft 200%	2	2·03	9·9	1·129	4·975	0·298	0·345	0·426	0·545
46	El Centro 50%	4	2·11	17·7	0·474	3·209	0·156	0·170	0·221	0·282
47	El Centro 100%	4	2·11	17·7	0·948	6·447	0·304	0·346	0·476	0·591
48	Taft 100%	4	2·11	17·7	0·561	2·494	0·145	0·161	0·208	0·246
49	Taft 200%	4	2·11	17·7	1·130	4·947	0·299	0·324	0·383	0·464

Table IV (continued)

Test	Excitation	DMP	System parameters		Peak shear force/weight			Peak drift/height (%)			Peak drift† height (%)
			f (Hz)	ξ (%)	1st story	2nd story	3rd story	1st story	2nd story	3rd story	1st story
27	El Centro 33·3%	0	2·00‡	1·74‡	0·220	0·199	0·139	0·976	1·069	0·769	—
28	El Centro 50%	0	2·00‡	1·74‡	0·295	0·272	0·195	1·386	1·498	1·073	—
29	Taft 100%	0	2·00‡	1·74‡	0·255	0·200	0·185	1·161	1·077	0·911	—
30	El Centro 50%	6	2·03	19·4	0·138	0·108	0·068	0·489	0·510	0·281	0·471
31	El Centro 100%	6	2·03	19·4	0·261	0·208	0·123	0·993	0·998	0·600	0·943
32	El Centro 150%	6	2·03	19·4	0·368	0·298	0·178	1·436	1·492	0·852	1·382
33	Taft 100%	6	2·03	19·4	0·120	0·104	0·059	0·425	0·463	0·253	0·399
34	Taft 200%	6	2·03	19·4	0·235	0·198	0·116	0·900	0·921	0·546	0·830
35	Taft 300%	6	2·03	19·4	0·343	0·288	0·171	1·407	1·369	0·819	1·270
36	Hachinohe 100%	6	2·03	19·4	0·256	0·201	0·111	1·036	0·963	0·575	0·957
37	Miyagiken 200%	6	2·03	19·4	0·254	0·202	0·114	0·947	0·963	0·610	0·890
38	Pacoima Dam 50%	6	2·03	19·4	0·275	0·224	0·125	1·106	1·017	0·629	1·003
39	Pacioma Dam 50% (H&V)	6	2·03	19·4	0·260	0·214	0·126	1·021	0·956	0·652	0·951
40	El Centro 100% (H&V)	6	2·03	19·4	0·260	0·202	0·130	0·998	1·029	0·588	0·941
41	Taft 200% (H&V)	6	2·03	19·4	0·236	0·195	0·117	0·929	0·931	0·531	0·829
42	El Centro 50%	2	2·03	9·9	0·196	0·159	0·100	0·806	0·865	0·548	0·750
43	El Centro 75%	2	2·03	9·9	0·282	0·233	0·142	1·210	1·292	0·785	1·124
44	Taft 100%	2	2·03	9·9	0·150	0·148	0·090	0·626	0·696	0·500	0·574
45	Taft 200%	2	2·03	9·9	0·296	0·279	0·182	1·247	1·431	0·983	1·181
46	El Centro 50%	4	2·11	17·7	0·159	0·132	0·094	0·540	0·660	0·465	0·520
47	El Centro 100%	4	2·11	17·7	0·314	0·256	0·197	1·142	1·279	0·933	1·081
48	Taft 100%	4	2·11	17·7	0·118	0·130	0·082	0·411	0·638	0·465	0·388
49	Taft 200%	4	2·11	17·7	0·253	0·249	0·155	0·949	1·208	0·829	0·887

DMP is the number of dampers.
f is the undamped frequency.
† indicates measured from component of damper displacement.
‡ for small amplitude of vibration.
H&V are the horizontal and vertical components.

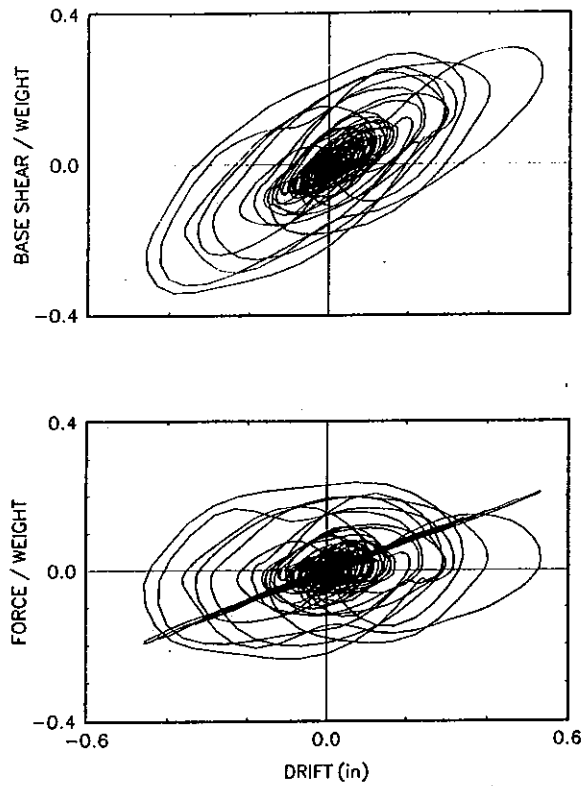

Figure 19. Experimental results for the one-story unstiffened structure with four dampers subjected to Taft 300% motion (1 in = 25·4 mm)

structure in comparison with the one-story structure is the result of lower damping in the bare frame of the three-story structure.

A comparison of responses of the three-story structure both with and without fluid dampers is presented in Figure 23. Clearly, the addition of fluid dampers resulted in a significant overall reduction of acceleration, story shear force and interstory drift.

A different comparison, presented in Figure 24, shows the response of the three-story structure both with and without dampers at two different levels of the same earthquake. The responses of the two systems are approximately the same for two significantly different levels of the same earthquake. It may be stated that, for this particular earthquake, the addition of fluid dampers has increased the earthquake resistance of the moment resisting bare frame by three-fold. This is generally not the case, however, and may be seen by an inspection of acceleration spectra of the input motion which shows that the reduction achieved by increasing damping from 5 to 20% of critical depends on the period of the structure and the frequency content of the excitation.

In Figure 24, the base shear force in the damped structure is larger than that of the undamped structure despite the overall lower accelerations. This is explained by considering the differences in the contribution of the higher modes of the two systems. In the undamped structure, the peak values of floor acceleration occur at different times as a result of contributions from the higher modes. In the damped structure, higher modes are almost completely suppressed and the peak values of floor accelerations occur at almost identical times.

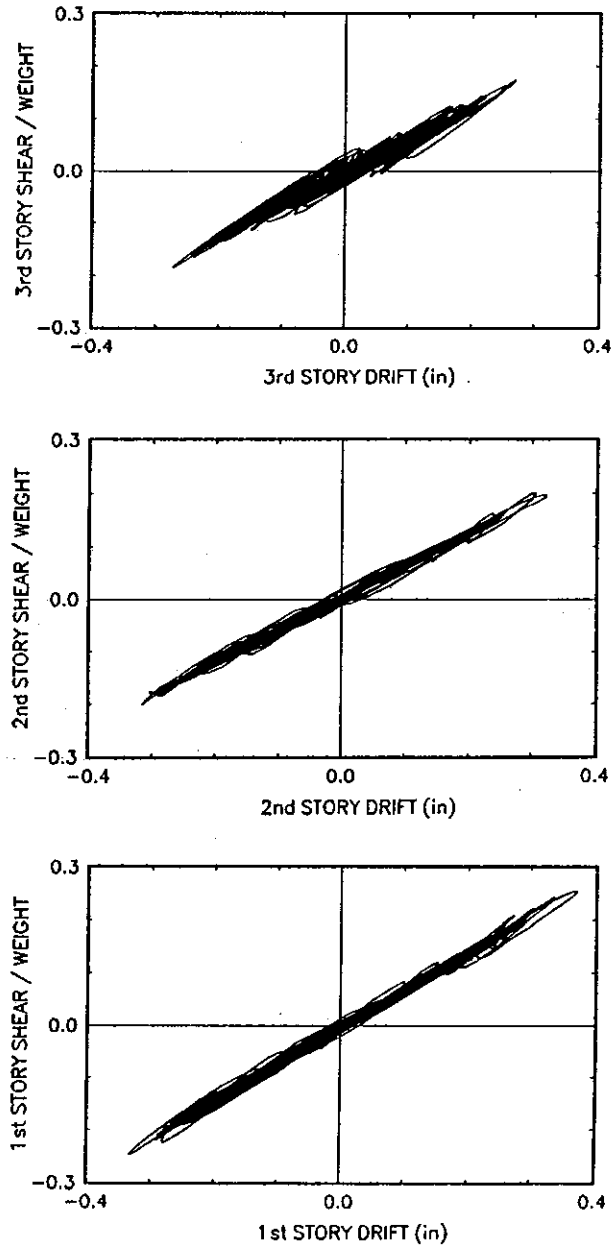

Figure 20. Experimental results for the three-story structure with no dampers subjected to Taft 100% motion (1 in = 25·4 mm)

An observation to be made from Tables II and IV is the effect that the vertical ground motion has on the response of the damped structure. The response, in terms of story drifts and shear forces, is affected. The effect is either a minor mixed increase and decrease of various response quantities or a minor net reduction of response. In general, this effect appears to be negligible.

The effect of fluid dampers on the behavior of a structural system to which they are attached

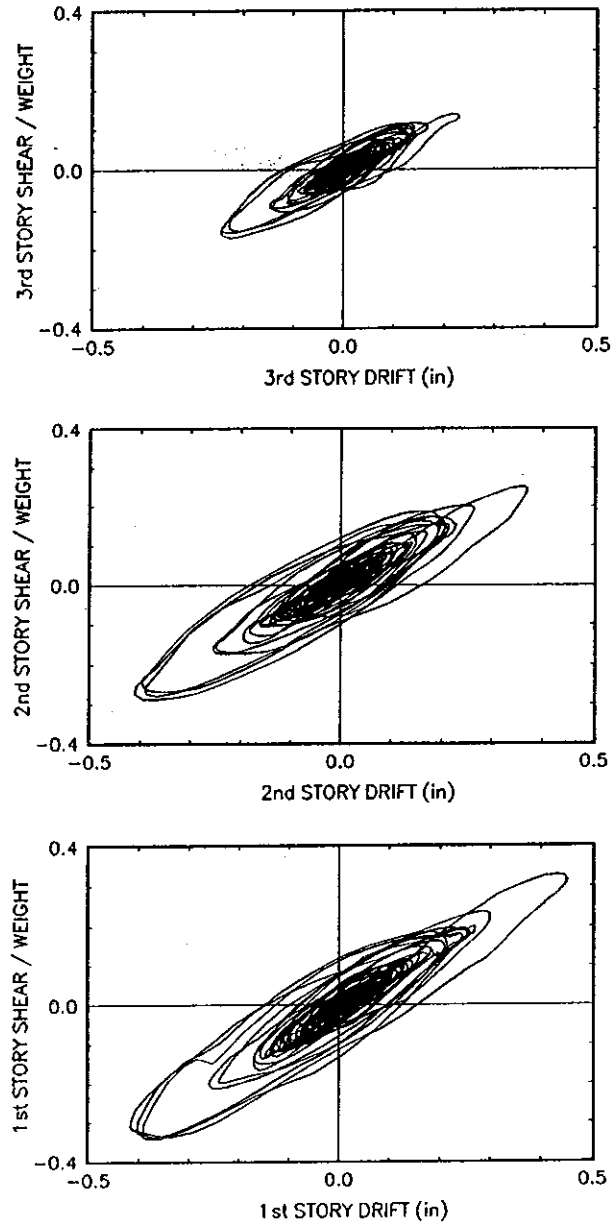

Figure 21. Experimental results for the three-story structure with six dampers subjected to Taft 300% motion (1 in = 25·4 mm)

is vividly illustrated in graphs of the time history of the energy dissipated by various mechanisms in the structure. Figure 25 shows energy time histories for the one-story structure subjected to the Taft 100% motion. The energies were calculated from the equation of motion after multiplication by du and integration over the time interval 0 to t. The result is[17]

$$E = E_k + E_s + E_h + E_d \tag{16}$$

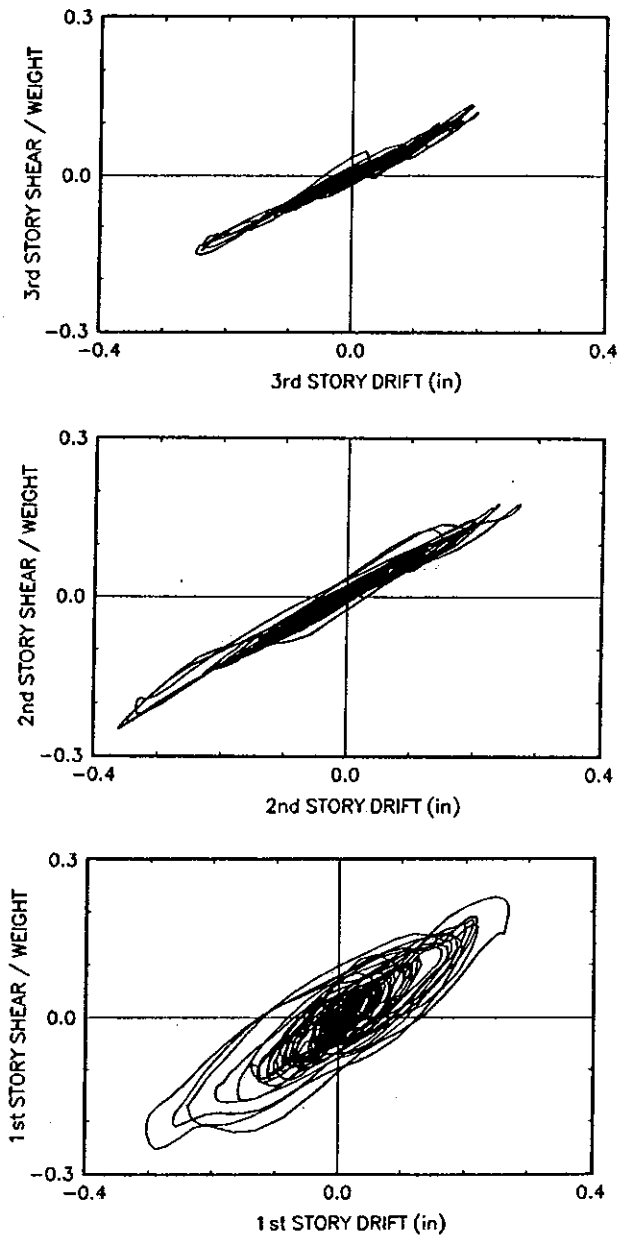

Figure 22. Experimental results for the three-story structure with four dampers (installed at the first story only) subjected to Taft 200% motion (1 in = 25·4 mm)

where

$$E = \int_0^t m(\ddot{u} + \ddot{u}_g)\, du_g \tag{17}$$

is the absolute energy input,

$$E_k = \tfrac{1}{2}m(\dot{u} + \dot{u}_g)^2 \tag{18}$$

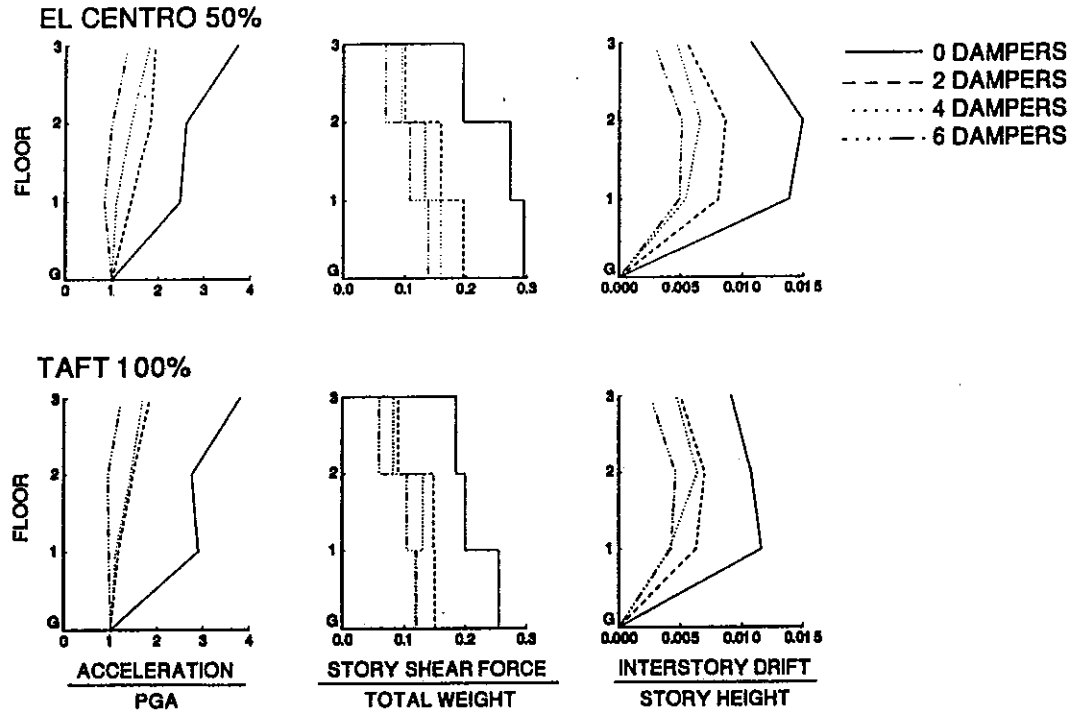

Figure 23. Acceleration, story shear and interstory drift profiles of three-story structure

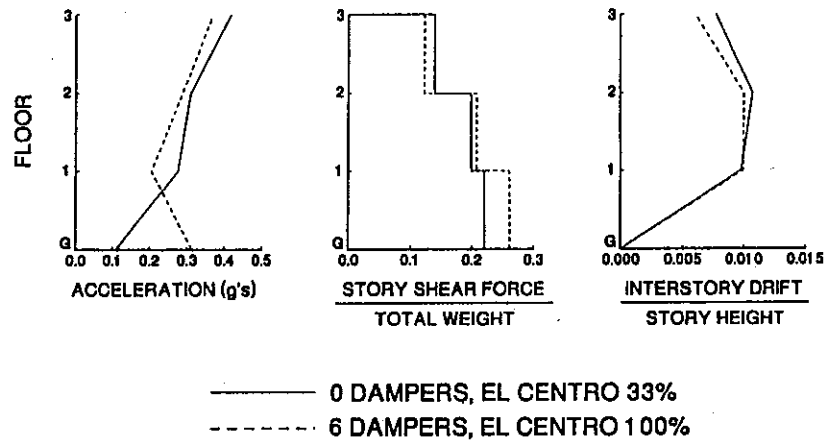

Figure 24. Comparison of response profiles for two different levels of the same earthquake

is the kinetic energy,

$$E_s = \tfrac{1}{2}ku^2 \tag{19}$$

is the recoverable strain energy,

$$E_d = \int_0^t \eta P_d \, du \tag{20}$$

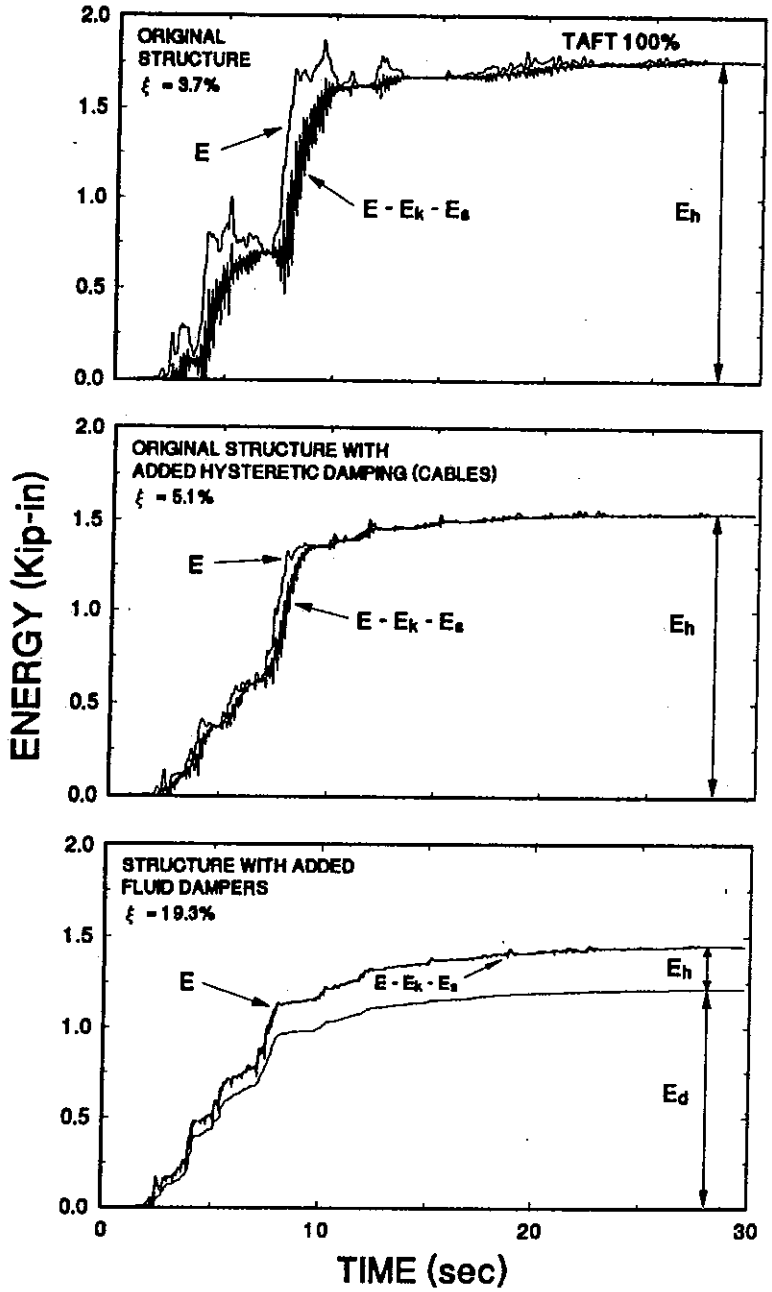

Figure 25. Energy time histories in one-story stiffened structure subjected to Taft 100% motion (1 kip ≡ 4·45 kN; 1 in = 25·4 mm)

is the energy dissipated by the fluid dampers, and E_h is the energy dissipated by other mechanisms in the structural frame (by viscous and hysteretic actions).

Figure 25 demonstrates a reduction of the absolute input energy with the addition of fluid dampers. Furthermore, the kinetic and strain energies are reduced. This demonstrates the

reduction of structural deformation. However, the most beneficial effect is the significant reduction of the energy dissipated in the structural frame in exchange for energy dissipation by the fluid dampers.

The three-story structure was tested in two different configurations. In the first, fluid dampers were placed at all stories (the case of six dampers). In the second, fluid dampers were placed only at the first story (the cases of 2 and 4 dampers). The primary effect of the difference in configuration was that damping in the fundamental mode varied from 9·9% (two dampers) to 17·7% (four dampers) to 19·4% of critical (six dampers). The secondary effect was substantial differences in the higher mode characteristics of the three systems.

In terms of the response of the three systems, Figure 23 provides a comparison of the systems for two earthquakes. Evidently, the concentration of the fluid dampers at one level did not have any adverse effect. The observed differences in the response of the three systems is just a result of a difference in the damping of the fundamental mode.

It should be noted that, in general, this behavior can be achieved by placing fluid dampers at those stories where the largest interstory velocity is expected. For response primarily in the first mode, this occurs at the story with maximum drift in the mode shape. In effect, increases in damping may be achieved either by the distribution of several fluid dampers over the height of the structure, or by strategically placing larger dampers at a few locations. The only drawback of such an approach is the development of larger forces at a few joints and the reduction in damper redundancy.

6. COMPARISON WITH OTHER ENERGY ABSORBING SYSTEMS

Direct comparison of responses of different structural systems to earthquakes is very difficult. Typically, a relatively small difference in the period of the structure may lead to dramatic changes in the response when the spectrum of the excitation exhibits significant changes in the range of periods containing the respective fundamental periods.

However, comparisons of indirect response quantities, such as the ratios of a particular response quantity in the damped structure with the same quantity in the undamped structure, may provide some limited insight into the behavior of various energy absorbing systems.

For this, we utilize recorded ratios of peak drift responses, RD, and peak base shear force, RBS. Table V provides a comparison of these quantities for various energy absorbing systems. The results in Table V demonstrate that all systems may produce comparable reductions in drift. Furthermore, fluid dampers produce reductions in base shear force that are not realized in the other energy absorbing systems. The reason for this behavior is the effectively viscous nature of fluid dampers. As stated earlier, this behavior has a further advantage in that the additional column axial forces are out-of-phase with the peak drift.[13]

Table V. Comparison of drift (RD) and base shear force (RBS) response ratios of various energy absorbing systems

System	RD	RBS	Reference
Viscoelastic dampers	0·5–0·9	~1	Aiken and Kelly, 1990
Friction dampers	0·5–0·9	~1	Aiken and Kelly, 1990
Yielding steel dampers	0·3–0·7	0·6–1·25	Whittaker *et al.* 1989
Fluid dampers	0·3–0·7	0·4–0·7	This study

In summary, the addition of fluid dampers significantly reduced both the peak base shear and peak drift in all tests performed. The simultaneous reduction of both of these response quantities is desirable in that the shear forces transmitted to the supporting columns are reduced and, at the same time, the non-structural elements are subjected to lower levels of relative displacement. With currently available seismic protection techniques, other than seismic isolation, it is often difficult to reduce both of these response quantities simultaneously.

7. COMPARISON WITH ACTIVE CONTROL

Active control systems are based on the development of external forces (e.g. those developed by actuators or actively moving masses) and have been studied extensively. Soong[18] demonstrated that the effect of the active control is primarily to modify the structural properties of stiffness and damping. In fact, successful experimental studies with an active tendon system[18,19] demonstrated that the primary effect of active control was to increase damping of the tested system with only minor or insignificant modification of stiffness.

In this respect, the achievements of active control may be reproduced and exceeded by fluid viscous dampers with the following additional advantages.

(a) *Low cost.* This is primarily achieved by utilizing the motion of the structure itself to generate the required damping forces rather than using other means external to the structural system (e.g. actuators).
(b) *Reliability.* Fluid dampers have demonstrated good performance over the last twenty years in military applications.
(c) *Power requirements.* Fluid dampers do not have external power requirements.
(d) *Longevity.* Fluid dampers have survived subjection to many years of continuous use in the harsh environment of military applications.

In Table VI, the experimental results obtained using the three-story model structure are compared with the results obtained using the same structure with an active control system.[18,19] This table compares the recorded response of the structure subjected to the 1940 El Centro, component S00E excitation when uncontrolled and when controlled by either an active tendon system or by fluid dampers. It is evident from this table that the effect of the active tendon system is only to modify damping, an effect that can be reliably produced by fluid dampers. Actually, the level of damping achieved by fluid dampers is such that, for this particular structure and excitation, the fluid dampers exhibit a clearly superior performance to that of active control.

8. ANALYTICAL PREDICTION OF RESPONSE

8.1. Equations of motion

The equations of motion of a base excited elastic multi-degree of freedom lumped mass structure with one degree of freedom per floor may be written in the following form:

$$[M]\{\ddot{u}\} + [C_u]\{\dot{u}\} + [K]\{u\} + \{P_d\} = -[M]\{1\}\ddot{u}_g \tag{21}$$

where $[M]$ is the mass matrix; $[C_u]$ is the damping matrix; $[K]$ is the stiffness matrix; $\ddot{u}_g$ is the ground acceleration; and $\{\ddot{u}\}$, $\{\dot{u}\}$ and $\{u\}$ are the vectors of relative acceleration, velocity and displacement of the degrees of freedom, respectively. Furthermore, $\{1\}$ is a vector which contains

Table VI. Comparison of response of tested three-story model structure

Control method	System parameters f (Hz)	System parameters ξ (%)	Excitation	Floor or story	Peak floor accel. (g)	Peak interstory drift / height (%)	Peak model accel. / PGA
Uncontrolled	2·24	1·62	El Centro	3	0·322	0·596	
	6·83	0·39	S00E	2	0·221	0·874	3·79
	11·53	0·36	PGA = 0·085 g	1	0·158	0·667	
Active tendon system	2·28	12·77	El Centro	3	0·200	0·405	
	6·94	12·27	S00E	2	0·138	0·592	2·35
	11·56	5·45	PGA = 0·085 g	1	0·139	0·392	
Uncontrolled	2·00	1·74	El Centro	3	0·585	1·073	
	6·60	0·76	S00E	2	0·410	1·498	3·73
	12·20	0·34	PGA = 0·157 g	1	0·389	1·386	
Six fluid dampers placed at all stories	2·03	19·40	El Centro	3	0·205	0·281	
	7·64	44·70	S00E	2	0·152	0·510	1·35
	16·99	38·04	PGA = 0·152 g	1	0·127	0·489	
Four fluid dampers placed at first story	2·11	17·70	El Centro	3	0·282	0·465	
	7·52	31·85	S00E	2	0·221	0·660	1·81
	12·16	11·33	PGA = 0·156 g	1	0·170	0·540	

units. Vector $\{P_d\}$ contains the horizontal components of damper forces acting on the floors:

$$\{P_d\} = \begin{Bmatrix} \eta_N P_N \\ \vdots \\ \eta_j P_j - \eta_{j+1} P_{j+1} \\ \vdots \\ \eta_1 P_1 - \eta_2 P_2 \end{Bmatrix} \tag{22}$$

where η_j is the number of dampers at the jth story ($j = 1, \ldots, N$) and P_j is the horizontal component of force in a damper at the jth story. It is assumed here that all dampers at a given story are identical.

The general constitutive equation describing the damper force P_j is (classical Maxwell model (9))

$$P_j + \lambda \frac{dP_j}{dt} = C_0 \cos^2 \theta_j \frac{d}{dt}(u_j - u_{j-1}) \tag{23}$$

in which θ_j is the angle of placement of damper j with respect to the horizontal and $u_0 = 0$ ($j = 1$).

8.2. Time history analysis

Application of Fourier transform to (21)–(23) results in

$$[S(\omega)]\{\bar{u}\} = -[M]\{1\}\bar{\ddot{u}}_g \tag{24}$$

in which the overbar denotes the Fourier transform and matrix $[S]$ represents the dynamic stiffness matrix:

$$[S(\omega)] = -\omega^2[M] + i\omega[C_u] + [K] + [D(\omega)] \tag{25}$$

Matrix $[D]$ contains the contribution of the damper forces to the dynamic stiffness matrix.

The construction of matrix [D] is given below for two of the three tested configuratons of the three-story structure depicted in Figure 12. It should be noted that all dampers are identical.

$$[D] = \frac{i\omega}{1 + i\omega\lambda}[C] \tag{26}$$

where for the case of two dampers at the first story

$$[C] = \begin{bmatrix} 0 & 0 & 0 \\ 0 & 0 & 0 \\ 0 & 0 & C_1 \end{bmatrix} \tag{27}$$

and for the case of six dampers

$$[C] = \begin{bmatrix} C_3 & -C_3 & 0 \\ -C_3 & C_2 + C_3 & -C_2 \\ 0 & -C_2 & C_1 + C_2 \end{bmatrix} \tag{28}$$

In the above equations,

$$C_i = 2C_0 \cos^2 \theta_i; \quad i = 1, 2 \text{ and } 3 \tag{29}$$

where C_0 is the damping constant of one fluid damper.

The Fourier transform of (23) is

$$\bar{P}_j = \frac{i\omega C_0 \cos^2 \theta_j}{1 + i\omega\lambda} (\bar{u}_j - \bar{u}_{j-1}) \tag{30}$$

Now (24) and (30) may be solved numerically by employing the discrete Fourier transform method:[20]

$$\{u(t)\} = \frac{-1}{2\pi} \int_{-\infty}^{\infty} [S]^{-1}[M]\{1\}\bar{\ddot{u}}_g e^{i\omega t} d\omega \tag{31}$$

$$P_j(t) = \frac{1}{2\pi} \int_{-\infty}^{\infty} \bar{P}_j e^{i\omega t} d\omega \tag{32}$$

Relative acceleration vectors are determined by an expression identical with (31) but with the term $-\omega^2$ multiplying the inverse of the dynamic stiffness matrix, $[S]^{-1}$. The total acceleration vector, $\{\ddot{u}_t\}$, is then obtained from

$$\{\ddot{u}_t\} = \{\ddot{u}\} + \{1\}\ddot{u}_g \tag{33}$$

The computed total acceleration histories are used in the calculation of the story shear forces.

8.3. *Transfer functions*

Transfer functions are useful in the identification of the vibrational characteristics of structures. An acceleration transfer function is defined as the ratio of the Fourier transform of the total acceleration of a degree of freedom to the Fourier transform of the ground acceleration.

Defining the inverse of matrix $[S]$ as $[H]$, (24) may be solved for $\{\bar{u}\}$. Upon multiplication by $-\omega^2$, the Fourier transform of the relative acceleration vector is obtained:

$$\{\bar{\ddot{u}}\} = \omega^2[H][M]\{1\}\bar{\ddot{u}}_g \tag{34}$$

The transfer function of the jth degree of freedom is by definition

$$T_j = \frac{\bar{\ddot{u}}_g + \bar{\ddot{u}}_j}{\bar{\ddot{u}}_g} \tag{35}$$

or

$$T_j = 1 + \omega^2 \sum_{k=1}^{K} H_{jk}(\omega) m_k \tag{36}$$

where H_{jk} are elements of matrix $[H]$ and m_k is the lumped mass at the kth floor.

8.4. *Eigenvalue problem*

For the determination of frequencies and damping ratios of the damped structure, (21) and (22) with $\ddot{u}_g$ set equal to zero are written in the form

$$[B]\{\dot{Z}\} + [A]\{Z\} = \{0\} \tag{37}$$

where

$$\{Z\} = \begin{Bmatrix} \{\dot{u}\} \\ \{u\} \\ \{P_d\} \end{Bmatrix} \tag{38}$$

$$[B] = \begin{bmatrix} [M] & [0] & [0] \\ [0] & [I] & [0] \\ [0] & [0] & \lambda[I] \end{bmatrix} \tag{39}$$

$$[A] = \begin{bmatrix} [C_u] & [K] & [I] \\ -[I] & [0] & [0] \\ -[C] & [0] & [I] \end{bmatrix} \tag{40}$$

and $[I]$ is the identity matrix. For a solution of the form

$$\{Z\} = \{Z_0\}\, e^{\mu t} \tag{41}$$

where μ and $\{Z_0\}$ are the complex eigenvalue and eigenvector, respectively, (41) reduces to

$$[A]\{Z_0\} = -\mu[B]\{Z_0\} \tag{42}$$

This equation describes a generalized eigenvalue problem. The solution of this problem (see, for example, Reference 21) will result in values of the eigenvalue μ.

The frequency ω_k and damping ratio ξ_k of the kth mode of vibration are determined from

$$\omega_k = |\mu_k| \tag{43}$$

$$\xi_k = -\frac{\mathbb{R}(\mu_k)}{\omega_k} \tag{44}$$

where $|\cdot|$ stands for the modulus and $\mathbb{R}$ for the real part of μ.[13]

8.5. Response spectrum analysis

The formulation described in (21) to (44) is valid for the case in which the fluid dampers are modeled as Maxwell elements. However, it has been noted that the dampers exhibit purely viscous behavior for frequencies below a certain cut-off frequency. This behavior may be described by (21)–(44) by simply setting $\lambda = 0$. In this respect, a structure with added fluid dampers may be modeled as a non-proportionally viscously damped system. This enables the development of an approximate method of analysis using response spectra. The advantage of this method over a time history analysis is that it gives the peak response directly by use of the usual design specification (i.e. the design spectrum).

The application of the response spectrum analysis method requires estimates of the structural properties to be available. Approximate methods for the determination of the frequencies, mode shapes and damping ratios of non-classically damped structures have been successfully applied in problems involving soil–structure interaction.[22,23] Veletsos and Ventura[24] have presented a comprehensive treatment of the method.

The method starts with the assumption that frequencies and mode shapes of the non-

classically damped structure are identical with those of the undamped structure. Typically, these quantities are determined in a standard eigenvalue analysis.

The modal damping ratios are determined from an analysis involving energy considerations. The damping ratio in the kth mode of vibration may be expressed as

$$\xi_k = \xi_{\text{str}_k} + \frac{W_k}{4\pi L_k} \tag{45}$$

where ξ_{str_k} is the damping ratio due to damping inherent to the structure, W_k is the work done by the dampers in a single cycle of free vibration, and L_k is the maximum strain energy. W_k may be expressed as

$$W_k = \sum_j \int_0^{T_k} P_j \, \mathrm{d}(u_j - u_{j-1}) \tag{46}$$

where P_j is the horizontal component of the force in the dampers at the jth story, and u_j is the displacement of the jth floor. Using (23), W_k may be expressed as

$$W_k = \pi\omega_k \sum_j C_j \cos^2 \theta_j (\phi_j - \phi_{j-1})^2 \tag{47}$$

where ϕ_j is the modal displacement of the jth floor in the kth mode of vibration and ω_k is the frequency of vibration in the kth mode. Furthermore, C_j is the combined damping coefficient of the dampers at the jth story.

The maximum strain energy is equal to the maximum kinetic energy, so that

$$L_k = (KE)_{\text{MAX}} = \frac{1}{2} \sum_j m_j \phi_j^2 \omega_k^2 \tag{48}$$

Combining (45)–(48), the damping ratio of the structure in the kth mode of vibration is determined to be

$$\xi_k = \xi_{\text{str}_k} + \frac{1}{2} \frac{\sum_j C_j \cos^2 \theta_j (\phi_j - \phi_{j-1})^2}{\omega_k \sum_j m_j \phi_j^2} \tag{49}$$

It is clear from (49) that in order to have the greatest contribution to the modal damping ratio, the dampers should be placed at story levels where the modal interstory drift $(\phi_j - \phi_{j-1})$ is maximum.

8.6. *Comparisons with experimental results*

Comparisons of analytical and experimental story shear force versus story drift loops of the three-story structure under seismic excitation are presented in Figure 26. Furthermore, Figure 27 compares loops of the total axial damper force at the first story versus axial damper displacement in the three-story structure. The comparison shows good agreement. The analysis was based on the more general Maxwell model for the fluid dampers. However, time history results obtained by the simple viscous model ($\lambda = 0$) gave nearly identical results.[13]

Figures 28 and 29 compare analytical and experimental amplitudes of acceleration transfer functions of the tested three-story structure. The experimental functions were obtained in shake table testing of the model with a banded 0 to 20 Hz white noise input of 0·05 g peak acceleration. The good agreement between the experimental and analytical transfer functions confirms the

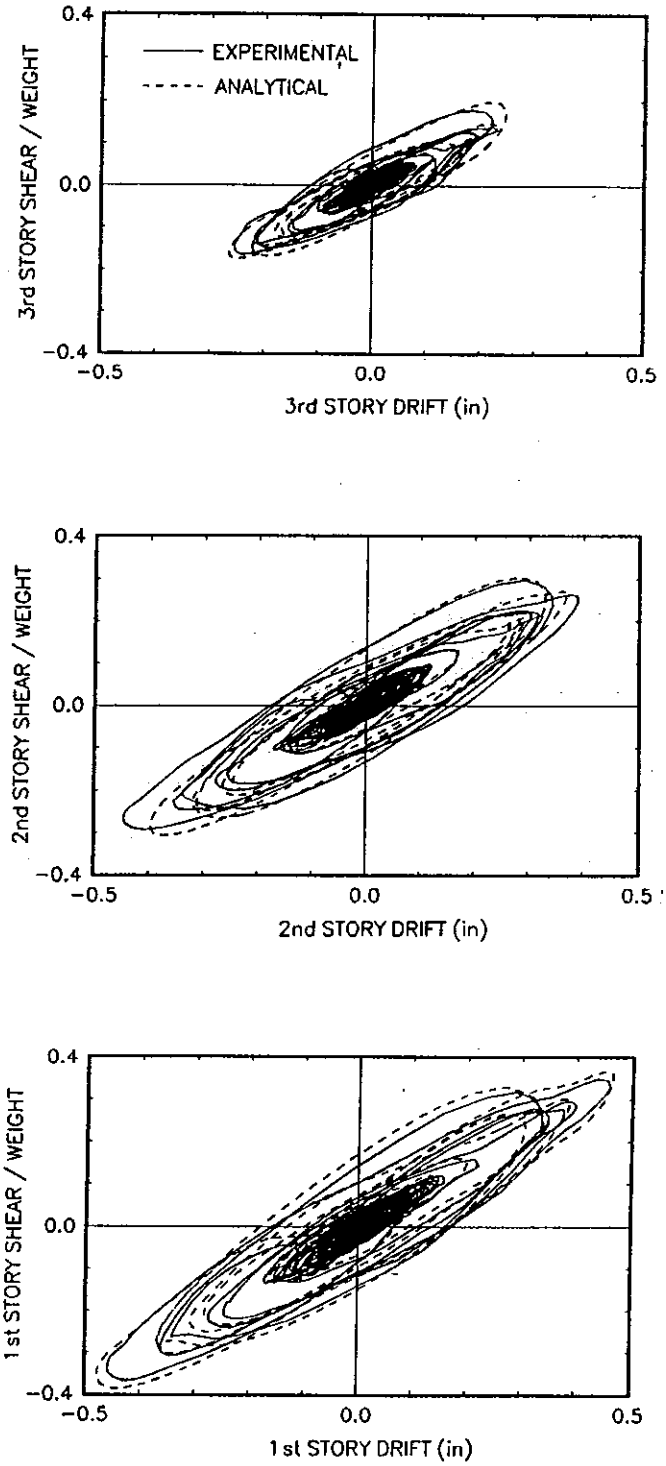

Figure 26. Comparison of experimental and analytical results for the three-story structure with six dampers subjected to El Centro 150% motion (1 in = 25·4 mm)

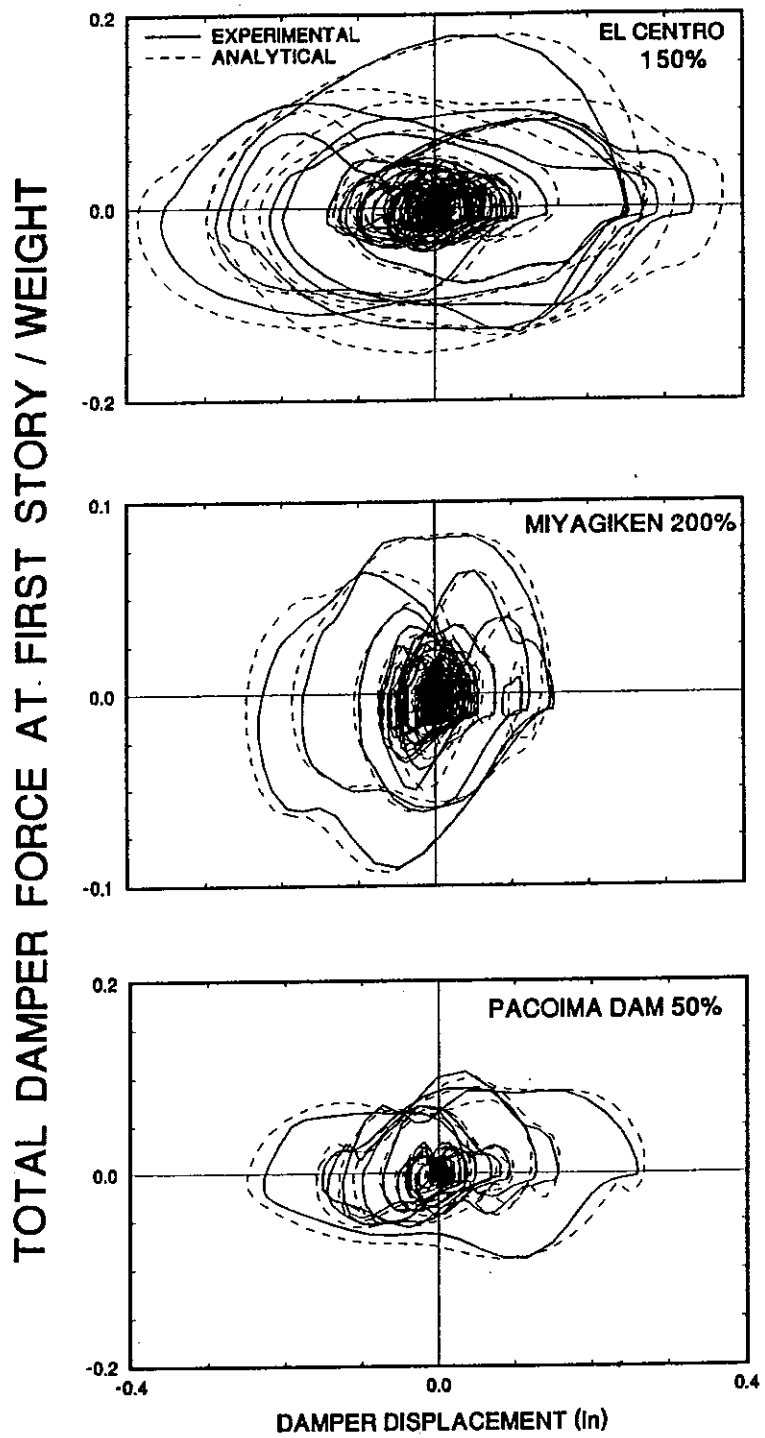

Figure 27. Comparison of experimental and analytical results for the dampers in the three-story structure with six dampers (1 in = 25·4 mm)

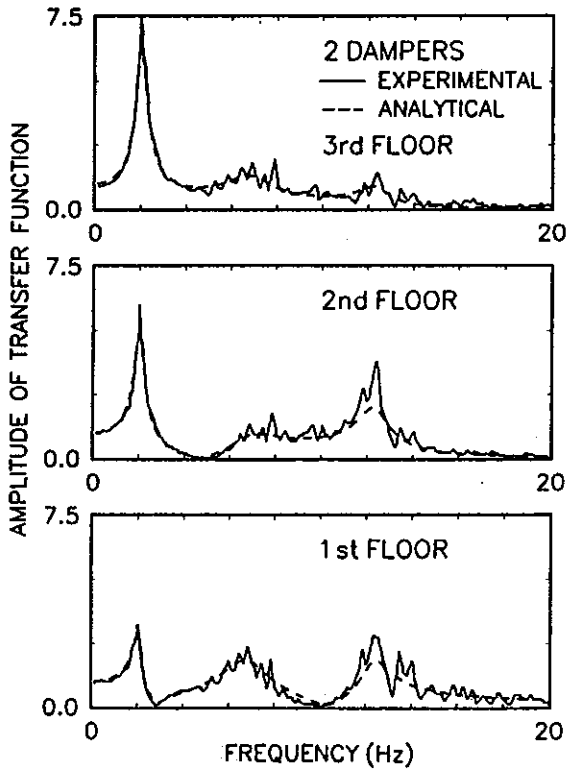

Figure 28. Comparison of analytical and experimental amplitudes of transfer functions of three-story structure with two dampers

accuracy of the analytical model. Thus, the verified analytical model may be used to extract the free vibrational characteristics. This approach was followed in the determination of the fundamental frequency and corresponding damping ratio reported in Tables II to IV.

The accuracy of the various methods presented for determining the damping ratios of the tested three-story structure is demonstrated in Table VII. The table includes the damping ratios calculated by the complex eigenvalue approach of (37)–(44) wherein the calibrated rigorous Maxwell model is utilized for the fluid dampers. The calculation was repeated by utilizing the

Table VII. Comparison of damping ratios of three-story model structure

Number of dampers	Rigorous method, Maxwell model			Rigorous method, viscous model			Energy approach, viscous model		
	Mode 1	Mode 2	Mode 3	Mode 1	Mode 2	Mode 3	Mode 1	Mode 2	Mode 3
2	0·099	0·147	0·050	0·100	0·154	0·049	0·100	0·149	0·051
4	0·177	0·319	0·113	0·183	0·326	0·081	0·183	0·291	0·098
6	0·194	0·447	0·380	0·193	0·428	0·490	0·193	0·428	0·490

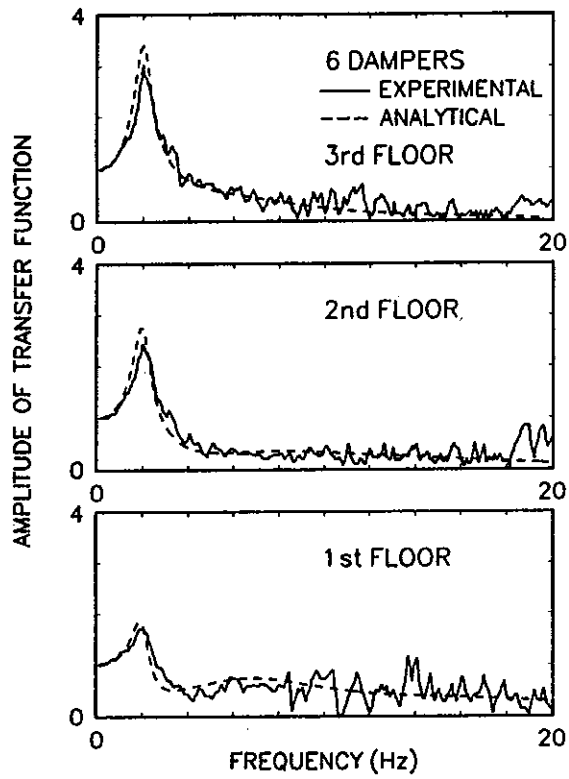

Figure 29. Comparison of analytical and experimental amplitudes of transfer functions of three-story structure with six dampers

simple viscous model and, thus, solving exactly the eigenvalue problem of the non-classically damped structure (λ was set equal to zero). Finally, the energy approach of (49) was employed.

The results demonstrate that the damping in the fundamental mode is predicted very well by the energy approach. In addition, the energy approach provides reasonable approximations to the damping ratios of the higher modes. The error in the calculation of the higher mode damping ratios is due to neglect of the stiffening effect of the tested fluid dampers at frequencies exceeding about 4 Hz.

Comparisons of the peak responses of interest in design (i.e. story shear forces and interstory drifts) are presented in Table VIII for the three-story structure with six dampers subjected to the El Centro 150% excitation. The peak response is given experimentally and analytically as calculated by time history analysis and by the response spectrum approach. For the application of the response spectrum approach, high damping displacement and acceleration spectra for the calculated damping by the energy approach were utilized.

The peak responses as determined by all four methods compare well. The prediction of story shear forces is very good. The simple response spectrum approach yields results that are accurate enough for design purposes.

Table VIII. Comparison of peak response to El Centro 150% excitation of three-story structure with six dampers as determined experimentally and by various analytical methods

Response	Experimental	Time history, Maxwell model	Time history, viscous model	Response spectrum approach
$\frac{\text{3rd Story shear}}{\text{Weight}}$	0·178	0·198	0·177	0·176
$\frac{\text{2nd story shear}}{\text{Weight}}$	0·298	0·307	0·295	0·294
$\frac{\text{1st Story shear}}{\text{Weight}}$	0·368	0·387	0·368	0·365
$\frac{\text{3rd Story drift}}{\text{Height}}$ (%)	0·852	0·889	0·876	0·896
$\frac{\text{2nd Story drift}}{\text{Height}}$ (%)	1·492	1·323	1·302	1·306
$\frac{\text{1st Story drift}}{\text{Height}}$ (%)	1·436	1·498	1·465	1·468

8.7. *Analysis by commercially available computer programs*

Any commercially available program capable of performing response spectrum analysis may be used to obtain the peak global response (accelerations, story drifts and story shear forces) of buildings with supplemental fluid dampers. The presented approximate energy method for computing damping ratios is useful in the construction of the applicable high damping response spectra. The only complexity in the application of this approach is that of constructing the high damping response spectra from the usually specified 5%-damped spectra. A recent study on this problem has been reported by Wu and Hanson.[25] However, it may be appropriate to include de-amplification factors of design spectra at high damping in future design requirements of structures with supplemental damping devices. This will ensure uniformity, reasonable conservatism and avoidance of gross errors.

The response spectrum approach is incapable of providing information on the forces in the dampers and the effect that these forces have on the structural members to which they are attached. To obtain this information, it is necessary to perform analysis with explicit modeling of individual dampers. For most practical applications, it is sufficient to model each fluid damper by the viscous model of (15). A variety of computer programs such as ANSYS,[26] ABAQUS[27] and DYNA3D,[28] are capable of modeling this behavior.

Explicit modeling of fluid dampers by more general models of viscoelasticity, such as the Maxwell model (9), is possible with computer programs ABAQUS[27] and DYNA3D.[28] In general, any linear viscoelastic force–displacement relation may be expressed in the form[14]

$$P = \int_0^t G(t - t')\dot{u}(t')\,dt' \tag{50}$$

where $G(t)$ is the relaxation modulus. For the Maxwell model (9), the relaxation modulus is

given by

$$G(t) = \frac{C_0}{\lambda} \exp\left[-\frac{t}{\lambda}\right] \tag{51}$$

The programs DYNA3D[28] and ABAQUS[27] have the capability for modeling relaxation moduli which includes the form of (51).

9. CONCLUSIONS

A combined experimental and analytical study of an energy absorbing system for structures consisting of fluid viscous dampers has been presented. Tests were conducted on one- and three-story model structures with various configurations of dampers. Dampers were placed either along the entire height of the three-story structure, or concentrated at the level of expected peak interstory drift. Tests were also conducted on the bare frame in a configuration resembling a moment resisting frame.

A comprehensive component test program on the fluid dampers was conducted. The test program evaluated the behavior of the dampers in a range of frequencies varying between essentially zero and 25 Hz, a range of amplitudes of essentially zero to 1 in (25·4 mm), and a range of temperatures between about zero and 50°C. The component tests resulted in a database of mechanical properties which enabled the development of a rigorous mathematical model.

The mathematical model was utilized in the time history analysis of the tested structures with very good results. Furthermore, simplified models and methods of analysis were developed, evaluated and shown to produce results in good agreement with the experiments.

The important conclusions of this study are summarized below.

(a) Fluid viscous dampers may be designed to exhibit a behavior that is essentially linear viscous for frequencies of motion below a certain cut-off frequency. For the tested damper this frequency was equal to about 4 Hz. Beyond this frequency the dampers exhibit viscoelastic behavior.

(b) Fluid dampers may be modeled over a wide range of frequencies by the classical Maxwell model. However, since the cut-off frequency is usually (or can be designed to be) above the frequencies of dominant modes of the structure, the dampers may be modeled as simple linear viscous dampers.

(c) Temperature has a minor effect on the behavior of the tested fluid dampers. Owing to a special design with a passive temperature-compensated orifice, the tested dampers exhibited variations of their damping constant from a certain value at room temperature (24°C) to +44% of that value at 0°C to −25% of that value at 50°C. This rather small change in properties over a wide range of temperatures is in sharp contrast to the extreme temperature sensitivity of viscoelastic dampers.

(d) The inclusion of fluid viscous dampers in the tested structures resulted in reductions in story drifts of 30% to 70%. These reductions are comparable to those achieved by other energy dissipating systems such as viscoelastic, friction and yielding steel dampers. However, the use of fluid dampers also resulted in reductions of story shear forces by 40% to 70%, while other energy absorbing devices were incapable of achieving any significant reduction.

(e) Fluid dampers are capable of achieving and surpassing the benefits offered by active control systems with the additional benefits of low cost, no power requirements, longevity and reliability.

(f) Owing to their viscous nature, fluid dampers reduce drifts and thus column bending moments, while introducing additional column axial forces which are out-of-phase with the bending moments. In effect, this behavior prevents the possibility of compression failure of weak columns in retrofit applications.

(g) Time history analyses of structures with added fluid dampers may be more conveniently performed by application of the discrete Fourier transform, since the dampers exhibit linear behavior. Such analyses were performed for the tested structure with the results being in good agreement with the results of the experiments.

(h) A simplified method for calculating the modal characteristics of structures with added fluid dampers was developed and verified. The method was used to obtain estimates of peak response of the tested structures by utilizing the response spectrum approach. The results obtained demonstrated that the simplified method is sufficiently accurate for design purposes.

REFERENCES

1. R. G. Tyler, 'Tapered steel energy dissipators for earthquake resistant structures', *Bulletin of the New Zealand National Society for Earthquake Engineering*, **11**(4), 282–294 (1978).
2. R. G. Tyler, 'Further notes on a steel energy-absorbing element for braced frameworks', *Bulletin of the New Zealand National Society for Earthquake Engineering*, **18**(3), 270–279 (1985).
3. A. S. Whittaker, V. V. Bertero, J. L. Alonso and C. L. Thompson, 'Earthquake simulator testing of steel plate added damping and stiffness elements', Report No. UCB/EERC-89/02, Earthquake Engineering Research Center, University of California, Berkeley, 1989.
4. I. D. Aiken and J. M. Kelly, 'Experimental study of friction damping for steel frame structures', *Proc. PVP Conference*, ASME 133, Pittsburgh, Pennsylvania, 1988, pp. 95–100.
5. I. D. Aiken and J. M. Kelly, 'Earthquake simulator testing and analytical studies of two energy-absorbing systems for multistory structures', Report No. UCB/EERC-90/03, Earthquake Engineering Research Center, University of California, Berkeley, 1990.
6. A. S. Pall and C. Marsh, 'Response of friction damped braced frames', *J. Struct. Engrg.*, **ASCE 108**, ST6, 1313–1323 (1982).
7. A. S. Pall, V. Verganelakis and C. Marsh, 'Friction dampers for seismic control of Concordia University Library Building', *Proc. 5th Canadian Conference on Earthquake Engineering*, Ottawa, Canada, 1987, pp. 191–200.
8. T. F. Fitzgerald, T. Anagnos, M. Goodson and T. Zsutty, 'Slotted bolted connections in aseismic design of concentrically braced connections', *Earthquake Spectra*, 5(2), 383–391 (1989).
9. A. Filiatrault and S. Cherry, 'Performance evaluation of friction damped braced steel frames under simulated earthquake loads', Report of Earthquake Engineering Research Laboratory, University of British Columbia, Vancouver, Canada, 1985.
10. K. C. Chang, T. T. Soong, S.-T. Oh and M. L. Lai, 'Seismic response of a 2/5 scale steel structure with added viscoelastic dampers', Report No. NCEER-91-0012, National Center for Earthquake Engineering Research, State University of New York, Buffalo, 1991.
11. F. Arima, M. Miyazaki, H. Tanaka and Y. Yamazaki, 'A study on building with large damping using viscous damping walls', *Proc. 9th World Conference on Earthquake Engineering*, Tokyo–Kyoto, Japan, 1988, Vol. 5, pp. 821–826.
12. R. C. Lin, Z. Liang, T. T. Soong and R. H. Zhang, 'An experimental study of seismic structural response with added viscoelastic dampers', Report No. NCEER-88-0018, National Center for Earthquake Engineering Research, State University of New York, Buffalo, 1988.
13. M. C. Constantinou and M. D. Symans, 'Experimental and analytical investigation of seismic response of structures with supplemental fluid viscous dampers', Report No. NCEER-92-0032, National Center for Earthquake Engineering Research, State University of New York, Buffalo, 1992.
14. R. B. Bird, R. C. Armstrong and O. Hassager, *Dynamics of Polymeric Liquids*, J. Wiley and Sons, New York, 1987.
15. N. Makris and M. C. Constantinou, 'Fractional-derivative Maxwell model for viscous dampers', *J. Struct. Engrg.*, ASCE **117**, ST9, 2708–2724 (1991).

16. T. T. Soong, A. M. Reinhorn and J. N. Yang, 'A Standardized model for structural control experiments and some experimental results', *Proc. Second International Symposium on Structural Control*, 1985, Waterloo, Canada, 1987.
17. C.-M. Uang and V. V. Bertero, 'Use of energy as a design criterion in earthquake-resistant design', Report No. UCB/EERC-88/18, Earthquake Engineering Research Center, University of California, Berkeley, 1988.
18. T. T. Soong, *Active Structural Control: Theory and Practice*, Longman, New York, 1990.
19. L. L. Chung, R. C. Lin, T. T. Soong and A. M. Reinhorn, 'Experimental study of active control of MDOF seismic structures', *J. Engrg. Mech.*, ASCE **115**, EM8, 1609–1627 (1989).
20. A. S. Veletsos and C. E. Ventura, 'Dynamic analysis of structures by the DFT method', *J. Struct. Engrg.*, ASCE **111**, ST2, 2625–2642 (1985).
21. International Mathematical Statistical Library (IMSL), *Subroutine GVCRG*, Houston, Texas, 1987.
22. M. Novak and L. El Hifnawy, 'Effect of soil–structure interaction on damping of structures', *Earthquake Engrg., Struct. Dyn.*, **11**, 595–621 (1983).
23. M. C. Constantinou, 'A simplified analysis procedure for base-isolated structures on flexible foundation', *Earthquake Engrg., Struct. Dyn.*, **15**, 963–983 (1987).
24. A. S. Veletsos and C. E. Ventura, 'Modal analysis of non-proportionally damped linear systems', *Earthquake Engrg., Struct. Dyn.*, **14**, 217–243 (1986).
25. J. Wu and R. Hanson, 'Study of inelastic spectra with high damping', *J. Struct. Engrg*, ASCE **115**, ST6, 1412–1431 (1989).
26. ANSYS, Swanson Analysis Systems, Inc., Houston, Pennsylvania, 1987.
27. ABAQUS, Hibbitt, Karlsson & Sorensen, Inc., Pawtucket, Rhode Island, 1989.
28. DYNA3D, University of California, Lawrence Livermore National Laboratory, 1991.